HHS Public Access

Author manuscript

Cell. Author manuscript; available in PMC 2020 May 16.

Published in final edited form as:

Cell. 2019 May 16; 177(5): 1217–1231.e18. doi:10.1016/j.cell.2019.03.036.

A forward chemical genetic screen reveals gut microbiota metabolites that modulate host physiology

Haiwei Chen[1], **Phu-Khat Nwe**[2], **Yi Yang**[1], **Connor E. Rosen**[1], **Agata A. Bielecka**[1], **Manik Kuchroo**[3], **Gary W. Cline**[4], **Andrew C. Kruse**[5], **Aaron M. Ring**[1], **Jason M. Crawford**[2,6], and **Noah W. Palm**[1,*]

[1]Department of Immunobiology, Yale University School of Medicine, New Haven, CT, USA

[2]Chemical Biology Institute and Department of Chemistry, Yale University, West Haven and New Haven, CT, USA

[3]Yale University School of Medicine, New Haven, CT, USA

[4]Department of Internal Medicine, Yale University School of Medicine, New Haven, CT, USA

[5]Department of Biological Chemistry and Molecular Pharmacology, Harvard Medical School, Boston, MA, USA

[6]Department of Microbial Pathogenesis, Yale University School of Medicine, New Haven, CT, USA

SUMMARY

The intestinal microbiota produces tens of thousands of metabolites. Here, we used host sensing of small molecules by G-protein coupled receptors (GPCRs) as a lens to illuminate bioactive microbial metabolites that impact host physiology. We screened 144 human gut bacteria against the non-olfactory GPCRome and identified dozens of bacteria that activated both well-characterized and orphan GPCRs, including strains that converted dietary histidine into histamine and shaped colonic motility; a prolific producer of the essential amino acid L-Phe, which we identified as an agonist for GPR56 and GPR97; and a species that converted L-Phe into the potent psychoactive trace amine phenethylamine, which crosses the blood-brain barrier and triggers lethal phenethylamine poisoning after monoamine oxidase inhibitor administration. These studies establish an orthogonal approach for parsing the microbiota metabolome and uncover multiple biologically relevant host-microbiota metabolome interactions.

[*]Correspondence: noah.palm@yale.edu, Lead Contact: Noah W. Palm.

AUTHOR CONTRIBUTIONS

HC designed the study, designed and performed experiments, analyzed all data and co-wrote the manuscript. PKN designed and performed all chemical characterization and quantitative metabolomics experiments and analyzed the resulting data. YY performed bioinformatic analyses. AAB performed whole genome sequencing. CER designed and performed experiments. MK performed bioinformatic analyses. GWC performed HPLC-based analyses of biogenic amine production by *M. morganii*. ACK assisted with experimental design and advised on data analysis and interpretation. AMR participated in designing the study and specific experiments. JMC designed and supervised chemical characterization and quantitative metabolomics experiments. NWP designed the study, supervised all research, participated in experimental design, and co-wrote the manuscript. All authors participated in editing the manuscript.

In Brief

Metabolites produced by the human microbiota are able to function as agonists for a range of G protein coupled receptors, making metabolome screening a useful tool to both de-orphan human GPCRs and identify metabolic exchanges between commensal microbes in the gut with effects on host physiology.

INTRODUCTION

The human gut microbiota produces thousands of unique small molecules that can potentially affect nearly all aspects of human physiology, from regulating immunity in the gut to shaping mood and behavior (Donia and Fischbach, 2015; Husted et al., 2017; Smith, 2013; Tan, 2017; Yano et al., 2015). These metabolites can act locally in the intestine or can accumulate up to millimolar concentrations in the serum (Donia and Fischbach, 2015; Fischbach, 2018; Pedersen et al., 2016; Perry et al., 2016). Recent studies employing state-of-the-art genomic and metabolomic approaches have begun to reveal the enormously complex intra- and inter-species microbial chemistries that potentially impinge on host physiology, as well as the impact of gut microbes on the processing of dietary small molecules and medical drugs (Dodd et al., 2017; Guo et al., 2017; Haiser et al., 2013; Larsbrink et al., 2014; Milshteyn et al., 2018). In addition, they underscore the importance of continuing to develop new approaches to explore the bioactive microbiota metabolome (Fischbach, 2018).

G-protein coupled receptors (GPCRs) are the largest family of membrane proteins encoded in the human genome (including over 350 conventional non-olfactory GPCRs), are critical sensors of diverse small molecules, and regulate various aspects of host physiology, including vision, mood, pain, and immunity (Wacker et al., 2017). Specific GPCRs are also known to sense microbial metabolites, such as microbiota-derived short-chain fatty acids (Husted et al., 2017; Tan, 2017), and recent studies have continued to reveal novel microbiota-derived GPCR ligands that can shape host physiology (Cohen et al., 2017; Cohen et al., 2015). Thus, the microbiota metabolome is a rich source of potential GPCR ligands.

Here, by building on recent developments in high-throughput screening of the complete GPCRome and activity-guided microbial metabolite identification approaches (Donia and Fischbach, 2015; Fischbach, 2018; Kroeze et al., 2015; Milshteyn et al., 2018), we developed a pipeline to screen human gut microbes for the ability to produce ligands that activate human GPCRs. In so doing, we established an orthogonal approach for elucidating biologically-relevant microbiota metabolite-host interactions and, in the process, uncovered multiple diet-microbe-host and microbe-microbe-host metabolic axes that shape both local and systemic host physiology.

RESULTS

A forward chemical genetic screen to identify bioactive microbiota metabolites

We set out to establish a high-throughput screening system to identify specific human gut microbes that produce agonists or antagonists of conventional GPCRs. We developed a

pipeline for parsing the microbiota metabolome based on the GPCR screening technology Parallel Receptor-ome Expression and Screening via Transcriptional Output-Tango (PRESTO-Tango) (Kroeze et al., 2015). This technology leverages the Tango β-arrestin recruitment assay to simultaneously measure the activation of nearly all non-olfactory GPCRs (Figure 1, S1A, B) (Barnea et al., 2008; Kroeze et al., 2015). We thus proceeded to exploit this assay to perform a broad-ranging screen of bioactive metabolites produced by diverse members of the human gut microbiota.

We previously assembled personalized gut microbiota culture collections from eleven inflammatory bowel disease patients through high-throughput anaerobic culture methods and next-generation sequencing (Palm et al., 2014). This collection yielded 144 unique bacterial isolates from five phyla, nine classes, eleven orders, and twenty families, as well as multiple strains that were assigned to the same species (Table S1). We cultured all members of our collection individually in a medium specialized for the cultivation of gut commensals (gut microbiota medium; GMM) (Goodman et al., 2011) and screened their supernatants for activation or inhibition of nearly all conventional GPCRs (as compared to media alone) using PRESTO-Tango (see methods for details) (Figure 1, 2).

Human gut microbes produce compounds that activate both well-characterized and orphan GPCRs

PRESTO-Tango screening revealed that bacterial-derived metabolite mixtures activated both well-characterized GPCRs as well as orphan receptors, including GPCRs from nearly every class (Figure 2). One specific pattern of activation tracked closely with gross phylogeny—Bacteroidetes and Proteobacteria potently activated the succinate receptor (Sucr1), while Firmicutes, Fusobacteria and Actinobacteria largely failed to activate this receptor (Figure 1 and Table S2). However, most activation patterns did not correlate with phylogeny, and multiple bacterial strains assigned to the same species exhibited unique GPCR agonist activities (Table S2). GMM alone also activated select GPCRs when compared to PBS, and supernatants from specific microbes sometimes reversed these effects either due to bacterial consumption of GPCR ligands in the media or bacterial production of GPCR antagonists (Table S3). Given the exquisite sensitivity of PRESTO-Tango, the veracity of all individual hits will need to be confirmed using alternative methods. Nonetheless, these data demonstrate that human gut microbes produce a remarkable array of GPCR ligands.

Human gut microbes produce compounds that activate aminergic receptors

Besides the succinate receptor, the next most prevalent class of GPCRs activated by gut commensals was the aminergic receptors, which are expressed in diverse tissues and cell types and regulate a variety of core physiological processes ranging from neurotransmission to immunity (Figure 2) (Albuquerque et al., 2009; Beaulieu and Gainetdinov, 2011; Thurmond et al., 2008). More than a dozen commensal supernatants activated the dopamine (DRDs) or histamine (HRHs) receptors (Figure 3A, S2). For example, ten Proteobacteria strains activated both DRDs and HRHs, including all eight *Morganella morganii* strains in our collection (Figure 3B, C, S2). In contrast, two *Lactobacillus reuteri* strains activated HRHs, while two distinct *L.reuteri* strains failed to activate HRHs despite displaying similar growth kinetics (Figure 3C, S2). Finally, one *Streptococcus* strain, but not two related

isolates of *Streptococcus*, activated DRD2–4, and two unclassified Enterobacteriaceae strains activated HRH1–4 and DRD2 but failed to activate other DRDs (Figure 3C, S2).

M. morganii was previously reported to produce various biogenic amines, including dopamine, tyramine, and phenethylamine (PEA) (Kim et al., 2000; Özoğul, 2004). We noted that all *M. morganii* supernatants activated DRD2–4, but not DRD1 and 5 (Figure 3A, B, S2). In contrast, dopamine itself activated all five dopamine receptors (Figure S1A). Therefore, we suspected that *M. morganii* might produce a metabolite that is structurally related to dopamine and can act as a selective ligand for DRD2–4 but not DRD1 or 5 (Figure S3A). We examined the ability of all possible upstream and downstream metabolites in the mammalian dopamine pathway to activate DRDs and found that PEA and tyramine showed identical activation patterns to *M. morganii* supernatant (Figure S3A–C). Accordingly, metabolomic analyses revealed that *M. morganii* produced only trace amounts of dopamine and no detectable tyramine, but instead secreted significant quantities of the potent trace amine PEA which, unlike dopamine and tyramine, can readily cross the blood-brain barrier (Figure 3D, S3D, E) (Oldendorf, 1971).

We next used the cyclic AMP response element-secreted human placental alkaline phosphatase (CRE-SEAP) assay to examine whether PEA and related chemicals also activate G proteins (in addition to β-arrestin) downstream of DRDs (Durocher et al., 2000). To facilitate use of the CRE-SEAP assay for GPCRs that couple to G proteins other than $G\alpha_s$, such as DRD2–4, we used a $G\alpha_s$-$G\alpha_o$ fusion protein (a kind gift of Stephen Liberles) to redirect DRD2–4 signaling to $G\alpha_s$ (Liberles and Buck, 2006). PEA activated G protein signaling downstream of all five dopamine receptors, which suggests that PEA is a full agonist for DRD2–4 and may be a biased agonist for DRD1 and 5 (Figure S4A, B).

Previous reports have also suggested that *M. morganii* produces histamine (Özoğul, 2004). We confirmed that *M. morganii* secreted significant amounts of histamine by ELISA and that our *M. morganii* strains encode a previously described histidine decarboxylase; furthermore, 48 of 49 previously deposited *M. morganii* strains also encoded this histidine decarboxylase (Figure 3E and Table S4, S5). Two *L. reuteri* strains and two Enterobacteriaceae strains from our collections also secreted histamine (Figure 3E). Based on whole genome sequencing, both the histamine-producing and non-histamine-producing strains of *L. reuteri* encoded an identical histidine decarboxylase proenzyme (Table S4, S5). Together, these data reveal that *M. morganii* secretes high levels of PEA, which acts as a potent dopamine receptor agonist, and that *M. morganii* and select strains of *L. reuteri* secrete histamine.

In mammals, PEA, dopamine, and tyramine are produced via decarboxylation of L-Phe, LDOPA, and L-Tyr, respectively, by the aromatic L-amino acid decarboxylase (AADC; Figure S3A) (Lovenberg, 1962). Thus, we tested whether *M. morganii* would similarly process these amino acids into their respective biogenic amines using a minimal medium (MM) lacking L-Phe, L-DOPA, L-Tyr, and L-His. Despite normal *M. morganii* growth in this medium, we could not detect any production of PEA, tyramine, dopamine, or histamine (Figure 3F). However, supplementation with L-Phe or L-His led to the production of high levels of PEA or histamine, and activation of DRD2–4 or HRH2–4 (Figure 3F, G). In

contrast, supplementation with LDOPA or L-Tyr failed to lead to the production of dopamine or tyramine, or activation of DRDs (Figure S4C). Thus, unlike mammalian AADC, *M. morganii* selectively converts L-Phe into PEA and cannot efficiently convert L-DOPA or L-Tyr into dopamine or tyramine. While it is currently unclear which genes are involved in production of PEA by *M. morganii*, whole genome sequencing revealed the presence of at least 17 decarboxylases that are shared between the two strains of *M. morganii* that we sequenced (Table S4, S5).

Microbiota-derived histamine promotes increased colonic motility through activation of the histamine receptors

All *M. morganii* strains and two *L. reuteri* strains in our collection generated histamine *in vitro* and supplementation with additional L-His significantly increased histamine production by these strains; in contrast, two distinct strains of *L. reuteri* failed to produce histamine regardless of supplementation with L-His (Figure 4A). To test whether *M. morganii* can also produce histamine *in vivo*, we colonized germ-free mice with two distinct mock communities containing 9 or 10 diverse human gut microbes or with *M. morganii* C135 with or without supplementation of 1% L-His in the drinking water to approximate an L-His-rich diet (*e.g.*, a meat-heavy diet) (Figure 4B). In addition, we monocolonized mice with two *L. reuteri* strains with divergent histamine production capabilities: *L. reuteri* C93, which produced significant histamine *in vitro*, and *L. reuteri* C88, which failed to produce histamine *in vitro*. Mice colonized with *M. morganii* C135 or *L. reuteri* C93 exhibited high levels of intestinal histamine production, while mice colonized with the two mock communities or *L. reuteri* C88 showed nearly undetectable intestinal histamine (Figure 4C). In addition, supplementation with dietary L-His increased histamine production in *M. morganii* monocolonized mice (Figure 4C). Finally, we also detected increased histamine in the serum of mice colonized with *M. morganii* (Figure S5A).

To determine the location of *M. morganii in vivo*, we used modified Niven's agar to enumerate *M. morganii* CFUs in gnotobiotic mice colonized with two mock communities of diverse human gut microbes plus *M. morganii* C135 (Mavromatis, 2002). We found that *M. morganii* constitutes approximately 5% of the microbiota in the context of a mock community, and primarily inhabits the cecum and colon (Figure S5C and Table S3). Notably, *M. morganii* also preferentially localizes in tissue- or mucus-associated niches in the colon in humans (Eun et al., 2016).

Oral gavage with histamine increases colon motility in rodents (Kim et al., 2011; Tyagi et al., 2009). We thus hypothesized that gut microbe-derived histamine might also increase intestinal motility. We monitored intestinal motility in gnotobiotic mice colonized with two mock communities (which do not produce histamine) or *M. morganii* C135 with or without administration of 1% L-His in the water and found that *M. morganii* induced a significant increase in fecal output, which was further increased upon supplementation with L-His (Figure 4D). Similarly, mice colonized with *L. reuteri* C93 exhibited increased fecal output as compared to mice colonized with *L. reuteri* C88 (Figure 4D).

To test whether *M. morganii* can impact host physiology in the context of a more diverse microbial community, we colonized germ-free mice with a mock community of nine human

gut microbes with or without *M. morganii* C135 and examined histamine accumulation in the gut and serum, as well as fecal output. Although the effects were less profound than those observed with monocolonizations, the addition of *M. morganii* to a mock community also led to an accumulation of histamine in the colon and serum (Figure 4E and S5D) as well as increased fecal output (Figure 4E). Finally, we found that treatment with histamine receptor antagonists could largely block the effects of *M. morganii* on fecal output despite accumulation of similar levels of histamine in the gut (Figure 4F).

To examine the potential importance of histamine production by *M. morganii* (or other microbes) in human physiology, we mined publicly available metagenomic and metabolomic data from the integrative Human Microbiome Project (see methods for details) to determine the relative abundance of histamine producing enzymes or histamine itself in microbiomes from patients with IBD versus healthy controls (Integrative, 2014). We found that CD patients exhibited an increased prevalence and abundance of histidine decarboxylase genes, including *M. morganii*-encoded histidine decarboxylase, as compared to healthy controls or UC patients (Figure 4G and Figure S5E), and that histamine itself was increased in fecal samples from CD and UC patients as compared to controls (Figure 4H). This observation is in line with previous studies demonstrating increased intestinal histamine in patients with IBD, but this was largely attributed to host-derived histamine production (Smolinska et al., 2014).

Together, these data demonstrate that *M. morganii* impacts intestinal motility through histamine secretion and activation of histamine receptors, that dietary histidine can enhance these effects, and that bacterial histidine decarboxylases (both generally and from *M. morganii*) are enriched in patients with CD.

M. morganii can trigger ‘phenethylamine poisoning’ when combined with monoamine oxidase inhibition

Unlike histamine, we observed only low levels of colonic PEA in *M. morganii* monocolonized mice (Figure 5A). One potential explanation for this observation is that many biogenic amines, including PEA, are rapidly degraded in the intestine by host monoamine oxidases (MAOs) (Glover, 1977). MAO inhibitors (MAOIs) were the first FDA-approved antidepressants (Fiedorowicz, 2004). Thus, to reveal the potential production of PEA *in vivo*, we treated germ-free mice or mice monocolonized with *M. morganii* C135 or a *Bacteroides thetaiotaomicron* strain (*B. theta* C34) that does not produce DRD agonists with the irreversible MAOI phenelzine. While colonic PEA remained undetectable in germ-free mice or mice colonized with *B. theta* even after phenelzine treatment, *M. morganii*-colonized mice treated with phenelzine exhibited high levels of colonic PEA (Figure 5A). *M. morganii*-colonized mice also became lethargic within days after MAOI treatment, and more than half of all *M. morganii*-colonized mice died by day seven post MAOI administration, while germ-free and *B. theta* C34-colonized mice remained healthy (Figure 5B). Morbidity and mortality after MAOI treatment correlated with elevated levels of PEA in the colon, serum, and brains of *M. morganii*-colonized mice (Figure 5C and S5F, G), and cecal and colonic contents, as well as serum and brain extracts from these mice also activated DRD2 (Figure 5D). Finally, mice colonized with a mock community plus *M.*

morganii also exhibited increased PEA in the colon and brain, as measured by DRD2 activation (Figure 5E). Together, these data show that *M. morganii*-derived phenethylamine can accumulate systemically and cross the blood-brain barrier in mice treated with MAOIs.

A unique *Bacteroides* isolate activates GPR56/AGRG1

We observed that specific bacterial supernatants activated select orphan GPCRs (Figure 6A). To confirm these hits, we repeated our PRESTO-Tango screening procedure using a richer culture medium (Gifu) that supports more robust growth of many of the human gut microbes in our collection. This modified procedure significantly expanded the number of positive hits against orphan GPCRs: 17 orphan GPCRs showed greater than four-fold activation in response to at least one bacterial supernatant (Figure 6B). Metabolites from a strain assigned to the species *B. theta* (*B. theta* C34) activated GPR56/AGRG1 under both culture conditions (Figure 6C). In contrast, other strains of *B. theta* as well as multiple related *Bacteroides* strains failed to activate GPR56/AGRG1 (Figure 6D) despite similar bacterial growth (Figure S6A).

The essential amino acid L-Phe activates GPR56/AGRG1 and GPR97/AGRG3

Since there was no known endogenous small molecule ligand for GPR56/AGRG1 (Purcell, 2018), we next attempted to identify the specific metabolite produced by *B. theta* C34 that activated GPR56/AGRG1. *B. theta* C34 supernatants were extracted and subjected to fractionation by reversed-phase HPLC and all fractions were analyzed for activity via GPR56-Tango (Figure 6E). High resolution mass spectrometry, NMR and coinjection analyses of the active fraction (F11) revealed the essential amino acid phenylalanine (Phe) as the primary constituent of F11 (Figure 6E and S6B) and structural characterization using advanced Marfey's analysis confirmed that L-Phe is the likely bioactive ligand (Figure S6C) (Bhushan and Bruckner, 2011). Accordingly, pure L-Phe and, to a lesser extent, L-Tyr stereoselectively activated GPR56/AGRG1, while L-Trp and L-His, D-Phe, D-Trp, D-His and D-Tyr showed no activity (Figure 6F and S6D). We hypothesized that L-Phe and L-Tyr in the medium used for the Tango assay might obscure the full extent of GPR56/AGRG1 activation by L-Phe. Indeed, removal of endogenous L-Phe and L-Tyr from the culture medium greatly increased the sensitivity and magnitude of GPR56 activation by L-Phe and L-Tyr as measured by GPR56-Tango (Figure 6G and S6E); furthermore, GPR56 expression was essential for this response (Figure S6E). Finally, despite their differential secretion of L-Phe, the genomes of *B. theta* C34 and two strains of *Bacteroides* that failed to activate GPR56/AGRG1 all encoded the full suite of enzymes in the shikimate pathway that synthesize L-Phe (Table S4, S5).

Using the promiscuous $G\alpha_s$-$G\alpha_t$ and $G\alpha_s$-$G\alpha_o$ chimeras and the CRE-SEAP assay described above (Liberles and Buck, 2006), we found that L-Phe activated G protein-dependent signaling downstream of GPR56/AGRG1 (Figure 6H and Figure S6F); however, since high concentrations of L-Phe (>1mM) were required to activate GPR56/AGRG1, it remains unclear whether physiological concentrations of L-Phe will engage GPR56/AGRG1-mediated G protein signaling *in vivo*. GPR56/AGRG1 belongs to the adhesion GPCR family, whose members possess large extracellular domains that mediate interactions with a variety of protein ligands (Purcell, 2018). However, we found that the extracellular

domain of GPR56/AGRG1 is also required for L-Phe-induced activation of GPR56/AGRG1 (Kishore et al., 2016) (Figure S6E). Together, our data demonstrate that a unique strain of *B. theta* secretes high levels of L-Phe and that L-Phe is a novel agonist of the adhesion GPCR GPR56/AGRG1.

We next examined whether other orphan GPCRs might also respond to L-Phe by stimulating all adhesion and orphan GPCRs with pure L-Phe (Figure S7A). We found that GPR97/AGRG3 also responded to L-Phe and showed greater selectivity toward L-Phe than GPR56/AGRG1—L-Phe, but not L-Tyr, L-Trp, or L-His, activated GPR97/AGRG3 (Figure S7B). Like GPR56/AGRG1, the extracellular domain of GPR97/AGRG3 was required for its ability to respond to L-Phe (Figure S7C), and removal of L-Phe and L-Tyr from the medium increased the magnitude of activation of GPR97/AGRG3 by exogenous L-Phe (Figure S7B and S7D). Furthermore, L-Phe also activated G protein-dependent signaling downstream of GPR97/AGRG3 (Figure S7E). Notably, GPR56/AGRG1 and GPR97/AGRG3 are evolutionarily related (Figure S7F), which may explain their shared ability to detect L-Phe.

Bacterial metabolic exchange can contribute to *in vivo* production of phenethylamine

Our reductionist studies revealed that *B. theta* C34 produces large amounts of L-Phe while *M. morganii* C135 can process L-Phe into PEA. Thus, we wished to address whether these two bacteria might participate in an active metabolic exchange *in vivo*. Using a defined minimal bacterial medium that lacks L-Phe (standard amino acid complete medium or SACC; see methods) (Dodd et al., 2017; Lovitt et al., 1987), we observed that *B. theta* C34 can directly synthesize large amounts of L-Phe *in vitro* (Figure 7A, B). Furthermore, mice monocolonized with *B. theta* C34 and fed an L-Phe-deficient diet displayed significant intestinal accumulation of L-Phe as compared to GF mice (Figure 7C).

We next examined whether *M. morganii* would process *B. theta* C34-derived L-Phe into PEA *in vitro* and observed that *B. theta* C34-derived L-Phe was efficiently converted into PEA by *M. morganii* C135 (Figure 7D). To test whether metabolic exchange occurs *in vivo*, we colonized GF mice with either *M. morganii* C135 alone or with both *B. theta* C34 and *M. morganii* C135, fed these mice a simplified diet lacking L-Phe, and then treated them with phenelzine. Mice colonized with *M. morganii* C135 alone remained healthy and produced minimal PEA in the absence of dietary L-Phe (Figure 7E). In contrast, mice co-colonized with *B. theta* C34 and *M. morganii* C135 became lethargic by day 4 after MAOI treatment and exhibited significant accumulation of PEA (Figure 7E). This demonstrates that metabolic exchange between *B. theta* C34 and *M. morganii* C135 can contribute to the production of a bioactive trace amine that can have potent effects on systemic host physiology.

DISCUSSION

The overwhelming complexity of the gut microbiota metabolome often obscures facile recognition of chemical communication between microbes and their hosts (Donia and Fischbach, 2015; Fischbach, 2018). Here, we used host GPCR activation as a lens to detect bioactive metabolites produced by individual gut microbes. We found that dozens of phylogenetically diverse human gut bacteria produced small molecules that activated various

GPCRs, including both well-characterized GPCRs and orphan GPCRs. We observed patterns of metabolite production that were largely predictable based on phylogeny, as well as strain-specific differences within a given species. Our approach thus revealed a plethora of novel microbiota metabolite-GPCR interactions of potential physiological importance. For example, we uncovered a diet-microbe-host axis that influences intestinal motility through microbial production of histamine and a tri-partite microbe-microbe-host relationship that results in the production of the potent trace amine phenethylamine. These chemicals exerted profound effects on both local and systemic host physiology. Overall, our results further support the notion that human-associated microbes represent a remarkably rich source of small molecules that impact human biology.

Prior studies have employed functional metagenomic screens as well as bioinformatics- and bioassay-guided natural product discovery approaches to uncover novel microbial-derived ligands for host GPCRs, including orphans (*e.g.*, SCFA and GPR41 and 43, and commendamide and G2A and GPR119; (Brown et al., 2003; Cohen et al., 2017; Cohen et al., 2015; Le Poul et al., 2003); however, these approaches also have notable limitations (Donia and Fischbach, 2015; Milshteyn et al., 2018). For example, while functional metagenomic screens enable identification of novel biosynthetic gene clusters and their products from unculturable microorganisms, they are restricted in scope to contiguous biosynthetic gene clusters that are active in heterologous hosts, require large-scale library construction, and necessitate extensive follow up to identify specific host receptors that recognize novel bioactive compounds. Similarly, while bioassay-guided natural product discovery efforts enable identification of compounds produced by native sources that engage a specific receptor or pathway, their utility is largely restricted to cultivatable microorganisms and they typically examine only a single receptor or activity at a time. In contrast, the high-throughput functional profiling approach that we employ here enables simultaneous interrogation of hundreds of receptors and thousands of chemicals and is unconstrained by prior annotations of biosynthetic gene clusters or metabolites (although still dependent on microbial cultivation). We thus anticipate that future expansions of our overall approach will continue to uncover microbial metabolites that impact host physiology and reveal novel natural ligands for orphan receptors.

We were particularly interested in examining the possibility that the microbiota-derived GPCR agonists we identified *in vitro* would also shape host physiology *in vivo*. We found that histamine production by *M. morganii* or *L. reuteri* increased colonic motility, that feeding with exogenous histidine enhanced this phenotype, and that histamine receptor inhibition reversed these effects. Since fecal output can be impacted by multiple factors (*e.g.*, fluid secretion and modulation of the enteric nervous system), future studies will be necessary to determine the mechanistic basis of this phenotype. *M. morganii* monocolonized mice also exhibited elevated levels of serum histamine, indicating a potential systemic role for microbiota-derived histamine. Notably, a recent study found that *M. morganii* relative abundance was increased in asthmatics as compared to healthy controls (Barcik et al., 2016). Finally, we found that histamine decarboxylases (specifically from *M. morganii*) are enriched in patients with Crohn's disease, which suggests that histamine production by the microbiota may directly impact IBD (Smolinska et al., 2014).

We found that all of our isolates of *M. morganii* produced PEA *in vitro* and that *M. morganii* monocolonized mice treated with an MAOI exhibited systemic accumulation of PEA and mortality. PEA is a potent neuroactive chemical that, unlike dopamine and tyramine, can readily cross the blood-brain barrier (Oldendorf, 1971). The effects of PEA are thought to be mediated primarily through activation of trace amine-associated receptors and subsequent release of norepinephrine and dopamine (Borowsky et al., 2001; Bunzow, 2001; Sotnikova et al., 2004). However, our studies suggest that PEA can also act as a full agonist for DRD2–4 and potentially a biased agonist for DRD1 and 5. While MAOIs were the first FDA-approved antidepressants (Ramachandraih, 2011), their current usage is limited due to dangerous diet- and drug-drug interactions (Fiedorowicz, 2004). Nonetheless, MAOIs remain an important treatment option for patients with refractory depression and other psychiatric disorders (Fiedorowicz, 2004). Since PEA enhances mood and can readily cross the blood-brain barrier (Irsfeld et al., 2013), our findings imply that inter-individual variability in microbial production of PEA could potentially explain the variable efficacy of MAOIs on depression.

Our studies also uncovered a specific *Bacteroides* strain that produces high levels of the essential amino acid L-Phe and revealed that L-Phe activates the orphans GPR56/AGRG1 and GPR97/AGRG3. These findings raise multiple intriguing possibilities. GPR56/AGRG1 is highly expressed in the small intestine and human pancreatic islets (Amisten et al., 2013; Duner et al., 2016), and L-Phe concentrations in the jejunum can reach concentrations up to 2 mM after a meal (Adibi, 1973). Thus, GPR56/AGRG1 may act as a nutrient sensor to regulate digestion and satiety. In addition, although L-Phe concentrations in the serum are typically well below the levels necessary to activate GPR56/97, patients with phenylketonuria (PKU) can exhibit serum L-Phe concentrations greater than 1 mM (Williams, 2008). Thus, it is also theoretically possible that GPR56/AGRG1 and/or GPR97/AGRG3 may be activated in extraintestinal tissues in PKU (*e.g.*, GPR56/AGRG1 is highly expressed in the central nervous system).

The natural microbiota metabolome results from a complex web of interactions between diverse microbial species and strains, environmental inputs (*e.g.*, diet), and host factors. Using a reductionist approach, we discovered two bacterial isolates that traffic in the same small molecule: a unique strain of *B. theta* that is a prolific producer of L-Phe and *M. morganii*, which converts L-Phe into PEA. These studies thus demonstrate that reductionist approaches can reveal metabolic exchanges that would be missed when examining endpoint microbiota metabolomes produced by complex mixtures of microorganisms. Understanding metabolic exchange networks will be essential to understand the effects of the microbiota metabolome on host biology under more physiological settings (*i.e.*, in the context of complete gut microbial communities) and to eventually leverage microbial chemistries for therapeutic benefit. Towards these ends, we examined the effects of *M. morganii* on host physiology in the context of a mock gut microbial community consisting of nine phylogenetically diverse human gut microbes. We found that *M. morganii* continued to exhibit measurable (albeit more modest) metabolite-dependent impacts on the host in the context of this simplified community. However, there are almost certainly other gut microbial community contexts where competition for ecological space or metabolic precursors (*e.g.*, L-His or L-Phe), or active degradation of *M. morganii*-derived metabolites

may reduce or eliminate the impact of *M. morganii* on the host (or, conversely, may enhance the effects of *M. morganii*).

Our studies underscore the role of dietary amino-acids (*e.g.*, L-His) in microbial production of biogenic amines. However, they also highlight the role of other members of the microbiota as sources of compounds that are often thought of as primarily derived from diet (*e.g.*, essential amino acids). This leads to the question of when microbial-produced amino acids may potentially supplement or even replace dietary amino acids in microbial biotransformations. We modeled the possibility that microbe-derived L-Phe can be biotransfored by *M. morganii* using a simplified diet that lacks L-Phe. However, bacterial L-Phe may also be important under more physiological conditions. For example, dietary amino acids are largely absorbed in the small intestine and thus free amino acid concentrations in the colon are often limiting (Adibi, 1973); also, low-protein diets and fasting can dramatically reduce intestinal amino acid availability (Pezeshki et al., 2016). Thus, microbial production of amino acids may play a critical role in the production of bioactive microbiota metabolites.

While our reductionist approach revealed multiple potentially physiologically important host-microbiota metabolome interactions, it also suffers from notable limitations. For example, microbial metabolite production varies substantially depending on the media used for cultivation, and *in vitro* monoculture conditions fail to capture metabolites that result from interactions with the host organism, biotransformations of compounds absent from the cultivation medium, or interactions with other microbes. Furthermore, the metabolite concentrations produced during *in vitro* cultivation may not reflect *in vivo* metabolite production. Finally, *in vitro* screens fail to reveal the natural tissue distributions of gut microbiota metabolites. Understanding these distributions will be particularly important for metabolites that activate host receptors that are expressed in diverse cell types and tissues. For example, histamine and dopamine receptors are expressed on cells as diverse as immune cells, central and peripheral neurons, smooth muscle, epithelial and endothelial cells, and in essentially all tissues including the gut, lung, and brain (Beaulieu and Gainetdinov, 2011; Jutel et al., 2009; Smolinska et al., 2014).

In conclusion, while the human gut microbiota metabolome is dauntingly complex and diverse, emerging approaches have begun to reveal key chemical interactions at the host-microbiota interface. We show here that high-throughput activity-based screening using potential host receptors as a lens can highlight physiologically relevant microbiota metabolites from complex metabolite mixtures. Such host-centric, functional profiling approaches can thus facilitate a mechanistic understanding of how we interact with and are affected by our microbial inhabitants, and have the potential to yield targeted therapeutic interventions aimed at the interface between indigenous microbes and their hosts.

STAR METHODS

See KRT Table Appended Separately

CONTACT FOR REAGENT AND RESOURCE SHARING

Further information and requests for resources and reagents should be directed to the Lead Contact, Noah W. Palm (noah.palm@yale.edu).

EXPERIMENTAL MODEL AND SUBJECT DETAILS

Mice.—6–12 week old germ-free wild-type C57Bl/6 mice were used in all experiments. Both male and female mice were used for these studies and mice were age and sex matched within each experiment (only one sex was used for each independent experiment). We did not observe any obvious sex-specific differences in *in vivo* phenotypes in any of these studies.

Bacteria.—All strains were cultured in gut microbiota medium (Goodman et al., 2011) or Gifu broth at 37 °C under anaerobic conditions and the identities of all strains were confirmed by 16S rRNA gene sequencing.

Media Formulations.—Custom (L-Phe- and L-Tyr-free) Dulbecco's Modified Eagle's Medium (DMEM) formulation

Ingredients	Concentration in Medium (g/L)
Inorganic Salts	
Calcium Chloride	0.2
Ferric Nitrate•9H_2O	0.0001
Magnesium Sulfate(anhydrous)	0.09767
Potassium Chloride	0.4
Sodium Bicarbonate	3.7
Sodium Chloride	6.4
Sodium Phosphate Monobasic(anhydrous)	0.109
Amino Acids	
L-Arginine•HCl	0.084
L-Cystine•2HCl	0.0626
L-Glutamine	0.584
Glycine	0.03
L-Histidine•HCl•H_2O	0.042
L-Isoleucine	0.105
L-Leucine	0.105
L-Lysine•HCl	0.146
L-Methionine	0.03
L-Phenylalanine	0
L-Serine	0.042
L-Threonine	0.095
L-Tryptophan	0.016
L-Tyrosine•2Na•2H_2O	0
L-Valine	0.094

Ingredients	Concentration in Medium (g/L)
Vitamins	
Choline Chloride	0.004
Folic Acid	0.004
myo-Inositol	0.0072
Niacinamide	0.004
D-Pantothenic Acid (hemicalcium)	0.004
Pyridoxine•HCl	0.004
Riboflavin	0.0004
Thiamine•HCl	0.004
Other	
Glucose	4.5
Phenol Red•Na	0.0159
Pyruvic Acid•Na	0.11

Minimal Medium

Ingredients	Concentration in Medium (g/L)
Resazurin	0.0001
$KH2PO_4$	2
$K2HPO_4$	2
$MgCl_2•6H_2O$	0.2
$(NH4)_2SO4$	5
L-Glycine	0.075
L-Valine	0.117
L-Leucine	0.131
L-Isoleucine	0.131
L-Methionine	0.149
L-Histidine	0
L-Arginine	0.174
L-Phenylalanine	0
L-Tyrosine	0
L-Tryptophan	0
$NaHCO_3$	2.5
Cysteine HCl	0.5
Glucose	3.603
Trace Mineral Supplement(g/L)	**10ml**
EDTA	0.5
$MgSO4•7H_2O$	3.0
$MnSO4•H_2O$	0.5
NaCl	1.0
$FeSO4•7H_2O$	0.1
$Co(NO_3)2•6H_2O$	0.1

Ingredients	Concentration in Medium (g/L)
$CaCl_2$ (anhydrous)	0.1
$ZnSO_4$•$7H_2O$	0.1
$CuSO_4$•$5H_2O$	0.010
$AlK(SO_4)_2$ (anhydrous)	0.010
H_3BO_3	0.010
Na_2MoO_4•$2H_2O$	0.010
Na_2SeO_3 (anhydrous)	0.001
Na_2WO_4•$2H_2O$	0.010
$NiCl_2$•$6H_2O$	0.020
Vitamin Supplement (mg/L)	**10ml**
Folic acid	2.0
Pyridoxine hydrochloride	10.0
Riboflavin	5.0
Biotin	2.0
Thiamine	5.0
Nicotinic acid	5.0
Calcium Pantothenate	5.0
Vitamin B12	0.1
p-Aminobenzoic acid	5.0
Thioctic acid	5.0
Monopotassium phosphate	900.0

Standard Amino Acid Complete (SACC) medium

Ingredients	Concentration in Medium (g/L)
Resazurin	0.0001
$KH2PO_4$	2
$K2HPO_4$	2
$MgCl_2$•$6H_2O$	0.2
$(NH4)_2$•SO4	5
L-Glycine	0.075
L-Valine	0.117
L-Leucine	0.131
L-Isoleucine	0.131
L-Methionine	0.149
L-Histidine	0.155
L-Arginine	0.174
L-Phenylalanine	0
L-Tyrosine	0.181
L-Tryptophan	0.204
$NaHCO_3$	2.5
Cysteine HCl	0.5

Ingredients	Concentration in Medium (g/L)
Glucose	3.603
Trace Mineral Supplement(g/L)	**10ml**
EDTA	0.5
$MgSO4•7H_2O$	3.0
$MnSO4•H_2O$	0.5
NaCl	1.0
$FeSO4•7H_2O$	0.1
$Co(NO_3)2•6H_2O$	0.1
$CaCl_2$ (anhydrous)	0.1
$ZnSO_4•7H_2O$	0.1
$CuSO_4•5H_2O$	0.010
$AlK(SO_4)_2$ (anhydrous)	0.010
H_3BO_3	0.010
$Na_2MoO_4•2H_2O$	0.010
Na_2SeO_3 (anhydrous)	0.001
$Na_2WO4•2H_2O$	0.010
$NiCl_2•6H_2O$	0.020
Vitamin Supplement (mg/L)	**10ml**
Folic acid	2.0
Pyridoxine hydrochloride	10.0
Riboflavin	5.0
Biotin	2.0
Thiamine	5.0
Nicotinic acid	5.0
Calcium Pantothenate	5.0
Vitamin B12	0.1
p-Aminobenzoic acid	5.0
Thioctic acid	5.0
Monopotassium phosphate	900.0

DATA AND SOFTWARE AVAILABILITY

Data deposition.—The raw sequence reads for all bacterial genomes have been deposited in the NCBI Sequence Read Archive (SRA) database in FASTQ format and genome assemblies have been deposited in NCBI genomes database in FASTA format. The accession number of the connected BioProject is PRJNA512876. The accession numbers for each raw sequence file are indicated in Table S4.

METHOD DETAILS

Bacterial growth conditions—For PRESTO-Tango screening, all commensals were cultured in gut microbiota medium or Gifu broth for 2 days in an anaerobic chamber (Coy) and commensal supernatants were sterilized by high-speed centrifugation and sterile filtration (0.22 μm). For *in vitro* studies, *M. morganii* was cultured in minimal medium

(MM), or MM with 10 mM L-Phe, 2.5mM L-Tyr, 10 mM L-DOPA, or 10mM L-His for 24 hours. Bacterial supernatants were analyzed by LC-MS.

PRESTO-Tango Assay—HTLA cells, a HEK293 cell line that stably expresses β-arrestin-TEV and tTA-Luciferase (a kind gift from Gilad Barnea, Brown University), were plated in 96-well tissue culture plates (Eppendorf) in DMEM containing 10% FBS and 1% Penicillin/Streptomycin. One day after plating (after reaching approximately 90% confluence), 200 ng per well GPCR-Tango plasmids (Kroeze et al., 2015) in 20 μl DMEM were mixed with 400 ng polyethylenimine (Polysciences) in an equal volume of DMEM and incubated for 20 minutes at room temperature before adding the transfection mixture to the HTLA cells. 16–24 hrs after transfection, medium was replaced with 180μl fresh DMEM containing 1% Penicillin/Streptomycin and 10mM HEPES and 20μl bacterial medium alone or bacterial supernatant. All bacteria were cultured in gut microbiota medium or Gifu under anaerobic conditions for 2 days and bacterial supernatant was isolated via high-speed centrifugation followed by filtration with a 0.22 μm filter. Bacteria that failed to reach an OD of 0.5 after 2 days or caused obvious cell toxicity (*e.g.*, *Clostridum perfringens* isolates) were excluded from further analysis. Supernatants were aspirated 16–24 hr after stimulation and 50 μl per well of Bright-Glo solution (Promega) diluted 20-fold with PBS containing 20mM HEPES was added into each well. After 20 min incubation at room temperature, luminescence was quantified using a Spectramax i3x (Molecular Devices). Activation fold for each sample was calculated by dividing relative luminescence units (RLU) for each condition by RLUs from media alone controls. No stimulation and bacterial media alone controls were included as separate conditions in each experiment to correct for day to day and experiment to experiment variability across the screen.

Histamine ELISA—All strains were cultured in gut microbiota medium with or without 1% L-His for 24 hours and supernatants were collected via high-speed centrifugation. Cecal and colonic contents and fecal samples were collected and weighed; all samples were suspended in PBS at a ratio of 1:2 (w/v) and were homogenized by vortexing. Serum and brains were collected, weighed and suspended in PBS at a ratio of 1:2 (w/v). Brains were homogenized by passing through a 21G needle fifty times. All samples were centrifuged and supernatants were collected for histamine ELISA according to the manufacturer's protocol.

Colonization of germ-free mice—Germ-free C57Bl/6 mice were colonized via oral gavage with 200μl of individual bacterial cultures or mixed bacterial consortia. Mock communities A and B consisted of the following taxa: Community A: *Bacteroides spp*; *P. distasonis*; *Peptoniphilus spp*; *B. ovatus*; *Clostridiales UC/UC*; *Lachnospiraceae UC/UC*; *C. stercoris*; *B. uniformis* and *Parabacteroides spp.*; and Community B: *Streptococcus spp*; *C. perfringens*; *B. fragilis*; *Erisipelotrichaceae spp*; *C. aerofaciens*; *Bacteroides UC*; *B. producta*; *Allobaculum spp* and *Oscillospira spp*. All strains were grown to roughly mid-log phase in GMM, mixed in equal ratios based on optical density, and then frozen at −80 °C in GMM containing 20% glycerol in rubber capped 2ml Wheaton vials until use. All gnotobiotic mice were maintained in Techniplast P Isocages and manipulated aseptically for the duration of the experiment. 16S rRNA gene sequencing of the V4 region to confirm colonization and microbial composition was performed essentially as described previously

(Palm et al., 2014) except that data processing and analysis was done using QIIME2-DADA2 (Caporaso et al., 2010).

Fecal output assay.—Individual mice were housed in an empty container (1/4 gallon) for 1 hour after which time the fecal pellets were counted and weighed. For mice fed with L-His, mice were given water containing 1% L-His *ad libitum* for 2 weeks before fecal output measurements. Based on an average water intake of 4 ml/ms/day combined with the existing dietary histidine present in conventional mouse chow (5 g/kg; Envigo), feeding of 1% L-His *ad libitum* in the water is equivalent to an overall histidine concentration of ~15g/kg in the diet. For reference, histidine rich foods such as soy protein, egg white, parmesan cheese, cured pork, and beef contain roughly 23, 20.5, 16, 16, and 14 g/kg of histidine, respectively (https://ndb.nal.usda.gov/ndb/nutrients/report/).

CRE-SEAP Assay.—96-well plates were pretreated with 30 μl poly-D-lysine (10ug/ml in water) and incubated at room temperature for 30 minutes. Plates were washed twice with 100 μl PBS and HEK293T were seeded in 100 μl DMEM+10% FBS+1% Penicillin/Streptomycin in each well. When cells were 90% confluent, plasmids were transfected using PEI reagent at a ratio of 1:2. For DRD1, DRD5 and TA1 (which couple to $G\alpha_s$ protein), HEK293T cells were transfected with 50 ng GPCR and 50 ng CRE-SEAP reporter plasmid per well; For DRD2, DRD3, DRD4, GPR56 and GPR97, cells were transfected with 50 ng GPCR, 50 ng CRE-SEAP reporter plasmid (BD Biosciences) and 2.5 ng $G\alpha_s$- $G\alpha_o$ or $G\alpha_s$-$G\alpha_t$ chimeras (a kind gift from Stephen Liberles, Harvard; (Liberles and Buck, 2006) per well. 6 hours after transfection, medium from the wells was replaced with 180 μl serum-free DMEM and 20 μl DMEM containing putative GPCR ligands was added to each well. After incubating for 48 hours at 37°C, followed by 2 hours of incubation at 70°C, supernatants from each well were mixed with an equal volume of 0.12 mM 4-methylumbelliferyl phosphate in 2 M diethanolamine bicarbonate, pH 10, and incubated at room temperature for 10 minutes. Fluorescence was measured using a SpectraMax plate reader (Molecular Devices).

Histamine Receptor Antagonist Treatment.—For histamine receptor antagonist treatment, 20 uM Desloratadine (HRH1 antagonist), Tiotidine (HRH2 antagonist), Iodophenpropit (HRH3 antagonist) and A987306 (HRH4 antagonist) were added to the drinking water. Colon motility was measured after one week of *ad libitum* treatment.

General Metabolomic Procedures.—NMR spectra were taken using an Agilent 600 MHz NMR system with a cryoprobe. High-resolution MS and tandem MS (MS/MS) data were obtained using an Agilent iFunnel 6550 ESIHRMS-QTOF (Electron Spray Ionization-High Resolution Mass Spectrometry-Quadrupole Time-of-Flight) instrument on Phenomenex Kinetex 5 μm C18 100Å (4.6 × 250 mm) columns. The Agilent 1260 Infinity system with a Phenomenex Kinetex 5 μm C18 100Å column (4.6 × 250 mm) or an Agilent Poroshell 120 EC-C18 2.7 μm (3.0 × 50 mm) column and a photodiode array (PDA) detector was used for routine sample analysis. An Agilent Prepstar HPLC system with an Agilent Polaris C18-A 5 μm (21.2 × 250 mm) column were used for sample fractionation and purification.

Metabolite Isolation and Purification.—*B. thetaiotaomicron* strain C11 was grown in 10 mL of gut microbiota medium under anaerobic conditions at 37°C for 24hr. Supernatant was harvested, lyophilized and extracted with 2mL methanol. The crude extract was then dried and fractionated using an Agilent Prepstar HPLC system with an Agilent Polaris C18-A 5 μm (21.2 × 250 mm) column. The gradient used was 10–50% acetonitrile in water (with 0.01% trifluoroacetic acid) for 30min, then 100% for 5min. The fractions, which were collected every minute, were dried, resuspended in PBS buffer, and tested for bioactivity using PRESTO-Tango. The active fraction was characterized using ESI-HRMSQTOF and NMR analyses (instruments listed as above). Stereochemistry was confirmed by advanced Marfey's analysis (Figure S5D) (Bhushan and Bruckner, 2011).

Metabolite Quantitation.—Electro Spray Ionization-Triple Quadrupole-Tandem Mass Spectrometry ESI-QQQ-MS/MS was run using Multiple Reaction Monitoring (MRM) mode. An Agilent 6490 ESI-QQQ-MS/MS instrument with a Phenomenex Kinetex 1.7 μm C18 100Å (100 × 2.10mm) column was used for quantitation and calibration. Each standard (L-Phenylalanine, Phenethylamine, Histamine, Tyramine, Dopamine) was optimized using an Agilent Mass Hunter Optimizer. A calibration curve for each standard was established using various concentrations (0 – 25μM range) in triplicate. The gradient constituted 10–100% acetonitrile in ddH_2O (with 0.1% Formic Acid), then a wash step with 100% acetonitrile. The triplicate data was then subjected to linear regression analysis to produce a linear calibration curve. Processing of the experimental samples involved lyophilization and extraction with 100% MeOH (20% volume of original culture volume) before injecting samples. Sample absorbance was subjected to linear calibration to calculate concentrations.

Whole-Genome Sequencing and Annotation, HMP2 Data Mining and Data Deposition.

Whole-genome sequencing.: Bacterial DNA was extracted using the DNeasy Ultraclean Microbial Kit (Qiagen) according to the manufacturer's instructions. Sequencing libraries were prepared using the Nextera XT library preparation kit (Illumina) according to the manufacturer's instructions and sequenced on a NovaSeq (2×150; Illumina).

De novo genome assembly.: Genome assembly and annotation were performed essentially as described in Dodd et al. (Dodd et al., 2017). Briefly, all Illumina paired-end reads were filtered and trimmed using Trimmomatic v.0.38 (Bolger et al., 2014) with the following parameters: ILLUMINACLIP: NexteraPE-PE.fa:2:30:12:1:true LEADING:3 TRAILING:3 MAXINFO:40:0.994 MINLEN:36. The four output files after trimming included two (forward and reverse) FASTQ files with paired reads and two FASTQ files with unpaired reads. All four files from each strain were assembled into contigs using SPAdes 3.13.0 (Nurk et al., 2013) with the default parameters for paired-end libraries. Genome coverage was calculated by BBMap (http://sourceforge.net/projects/bbmap/). Summary statistics for each genome assembly and alignment are shown in Table S3.

Genome annotation.: For each genome assembly, scaffolds longer than 2000 bp were uploaded to the Rapid Annotation using Subsystem Technology (RAST) server (Aziz et al., 2008) for annotation (using the default RASTtk pipeline). The annotated genomes were

downloaded as spreadsheets (Excel XLS format), and the summary of genome annotations as well as the detailed annotations for each strain are shown in Table S3.

HMP2 data acquisition and analysis.: Publicly available metagenome and metabolome data from the HMP2 were downloaded from The Inflammatory Bowel Disease Multi'omics Database (IBDMDB), which was funded by the NIH Human Microbiome Project NIDDK U54DE023798 (https://ibdmdb.org). The IBDMDB provides longitudinal meta'ome data on the microbiome of subjects with three clinical diagnoses: nonIBD, CD and UC. Raw metagenomic sequencing data was pre-processed and used to generate taxonomic and functional profiles by the HMP team. The pipeline employed two steps: (1) MetaPhlAn2 (Truong DT, 2015)-based taxonomic profiling, which uses clade-specific marker genes to identify species-level microbial taxa and their relative abundances using metagenomic data; and (2) HUMAnN2 (Franzosa EA, 2018)-based functional profiling. Briefly, HUMAnN2 implements a tiered search strategy to profile the functional content (gene family, functional pathway, *etc.*) of a meta'ome sample at species-level resolution. In the first tier, based on the known microbial species in a sample (as identified by MetaPhlAn2), HUMAnN2 constructs a custom gene sequence database for the samples by concatenating precomputed, functionally annotated pangenomes of detected species. In the second tier, nucleotide-level mapping of all reads against the sample's pangenome database is performed. In the final search tier, reads that do not align to an identified species' pangenome are then subjected to translated search against a comprehensive, non-redundant protein sequence database (UniRef90 or UniRef50). Per-gene alignment statistics are weighted based on alignment quality, coverage and sequence length to yield gene abundance values. Both taxonomic determinations and functional gene abundances are normalized as relative abundances to facilitate comparisons between samples with different sequencing depths.

The merged tables of taxonomic profiles (https://ibdmdb.org/tunnel/products/HMP2/WGS/1818/taxonomic_profiles.tsv.gz) and functional profiles (https://ibdmdb.org/tunnel/products/HMP2/WGS/1818/ecs.tsv.gz) from metagenomic analyses, the merged table from metabolomics analysis (https://ibdmdb.org/tunnel/products/HMP2/Metabolites/1723/HMP2_metabolomics.csv.gz), and the HMP2 metadata (https://ibdmdb.org/tunnel/products/HMP2/Metadata/hmp2_metadata.csv), were downloaded and analyzed to evaluate the distribution of abundance of histidine decarboxylase and histamine in this cohort. For participants whose clinical diagnosis changed during the course of the study, data points were assigned to the clinical diagnosis at the time of sample collection.

Quantification and Statistical Analysis.—Statistical analysis was performed using Graphpad Prism version 7.0. Data were assessed for normal distribution and plotted in the figures as mean ± SEM. No samples or animals were excluded from the analyses. One-way ANOVA and post hoc analysis with Tukey's test was used to compare the difference between treatment groups. Kaplan-Meier and Log rank analysis was used for survival experiments. Kruskall-Wallis with Dunn's multiple comparisons was used to analyze metagenomic and metabolomic data from the HMP; p-values for Kruskall-Wallis are approximated based on the chi-squared distribution and account for rank ties. Samples sizes

are indicated in each figure legend and significant differences are indicated in the figures by *p < 0.05, **p < 0.01, ***p < 0.001, ****p < 0.0001.

Supplementary Material

Refer to Web version on PubMed Central for supplementary material.

ACKNOWLEDGEMENTS

The authors thank members of the Palm laboratory for useful discussions and J. Henao-Mejia, A. Wang, and R. Medzhitov for critical reading of the manuscript. The NWP lab acknowledges support from Yale University School of Medicine and the Kingsley Award in Biomedical Research, the Helmsley Foundation, the Richard and Susan Smith Family Foundation, the Rainin Foundation, the Global Probiotics Council, the National Institutes of Health (K22 AI123477; R21 AI137935), TATA Sons Limited and Artizan Biosciences. The JMC lab acknowledges support from the Camille and Henry Dreyfus Foundation (TC-17–011), the Damon Runyon Cancer Research Foundation (DRR-39–16), the National Institutes of Health (1DP2-CA186575), the Burroughs Wellcome Foundation (1016720) and Yale University. The AMR lab acknowledges support for this work from an NIH Director's Early Independence Award (DP5-OD023088) and the Robert T. McCluskey Foundation.

DECLARATION OF INTERESTS

NWP is a co-founder of, consultant for, and receives research funding from Artizan Biosciences. HC, AMR, and NWP are inventors on a patent application based on these studies.

REFERENCES

Adibi S M. DW. (1973). Protein Digestion in Human Intestine as Reflected in Luminal, Mucosal, and Plasma Amino Acid Concentrations after Meals. The Journal of Clinical Investigation 52, 1586–1594. [PubMed: 4718954]

Albuquerque EX, Pereira EF, Alkondon M, and Rogers SW (2009). Mammalian nicotinic acetylcholine receptors: from structure to function. Physiol Rev 89, 73–120. [PubMed: 19126755]

Amisten S, Salehi A, Rorsman P, Jones PM, and Persaud SJ (2013). An atlas and functional analysis of G-protein coupled receptors in human islets of Langerhans. Pharmacol Ther 139, 359–391. [PubMed: 23694765]

Aziz RK, Bartels D, Best AA, DeJongh M, Disz T, Edwards RA, Formsma K, Gerdes S, Glass EM, Kubal M, et al. (2008). The RAST Server: rapid annotations using subsystems technology. BMC Genomics 9, 75. [PubMed: 18261238]

Bankevich A, Nurk S, Antipov D, Gurevich AA, Dvorkin M, Kulikov AS, Lesin VM, Nikolenko SI, Pham S, Prjibelski AD, et al. (2012). SPAdes: a new genome assembly algorithm and its applications to single-cell sequencing. J Comput Biol 19, 455–477. [PubMed: 22506599]

Barcik W, Pugin B, Westermann P, Perez NR, Ferstl R, Wawrzyniak M, Smolinska S, Jutel M, Hessel EM, Michalovich D, et al. (2016). Histamine-secreting microbes are increased in the gut of adult asthma patients. J Allergy Clin Immunol 138, 1491–1494 e1497. [PubMed: 27576125]

Barnea G, Strapps W, Herrada G, Berman Y, Ong J, Kloss B, Axel R, and Lee KJ (2008). The genetic design of signaling cascades to record receptor activation. Proc Natl Acad Sci U S A 105, 64–69. [PubMed: 18165312]

Beaulieu JM, and Gainetdinov RR (2011). The physiology, signaling, and pharmacology of dopamine receptors. Pharmacol Rev 63, 182–217. [PubMed: 21303898]

Bhushan R, and Bruckner H (2011). Use of Marfey's reagent and analogs for chiral amino acid analysis: assessment and applications to natural products and biological systems. J Chromatogr B Analyt Technol Biomed Life Sci 879, 3148–3161.

Bolger AM, Lohse M, and Usadel B (2014). Trimmomatic: a flexible trimmer for Illumina sequence data. Bioinformatics 30, 2114–2120. [PubMed: 24695404]

Borowsky B, Adham N, Jones KA, Raddatz R, Artymyshyn R, Ogozalek KL, Durkin MM, Lakhlani PP, Bonini JA, Pathirana S, et al. (2001). Trace amines: identification of a family of mammalian G protein-coupled receptors. Proc Natl Acad Sci U S A 98, 8966–8971. [PubMed: 11459929]

Brown AJ, Goldsworthy SM, Barnes AA, Eilert MM, Tcheang L, Daniels D, Muir AI, Wigglesworth MJ, Kinghorn I, Fraser NJ, et al. (2003). The Orphan G protein-coupled receptors GPR41 and GPR43 are activated by propionate and other short chain carboxylic acids. J Biol Chem 278, 11312–11319. [PubMed: 12496283]

Bunzow J S. MS; Arttamangkul S; Harrison LM; Zhang G; Quigley DI; Darland T; Suchland KL; Pasumanmula S; Kennedy JL; Olson SB; Magenis RE; Amara SG; Grandy DK. (2001). Amphetamine, 3,4-Methylenedioxymethamphetamine, Lysergic Acid Diethylamide, and Metabolites of the Catecholamine Neurotransmitters Are Agonists of a Rat Trace Amine Receptor. Molecular Pharmacology 60, 1181–1188. [PubMed: 11723224]

Callahan BJ, McMurdie PJ, Rosen MJ, Han AW, Johnson AJ, and Holmes SP (2016). DADA2: High-resolution sample inference from Illumina amplicon data. Nat Methods 13, 581–583. [PubMed: 27214047]

Caporaso JG, Kuczynski J, Stombaugh J, Bittinger K, Bushman FD, Costello EK, Fierer N, Pena AG, Goodrich JK, Gordon JI, et al. (2010). QIIME allows analysis of high-throughput community sequencing data. Nat Methods 7, 335–336. [PubMed: 20383131]

Cohen LJ, Esterhazy D, Kim SH, Lemetre C, Aguilar RR, Gordon EA, Pickard AJ, Cross JR, Emiliano AB, Han SM, et al. (2017). Commensal bacteria make GPCR ligands that mimic human signalling molecules. Nature 549, 48–53. [PubMed: 28854168]

Cohen LJ, Kang HS, Chu J, Huang YH, Gordon EA, Reddy BV, Ternei MA, Craig JW, and Brady SF (2015). Functional metagenomic discovery of bacterial effectors in the human microbiome and isolation of commendamide, a GPCR G2A/132 agonist. Proc Natl Acad Sci U S A 112, E4825–4834. [PubMed: 26283367]

Dodd D, Spitzer MH, Van Treuren W, Merrill BD, Hryckowian AJ, Higginbottom SK, Le A, Cowan TM, Nolan GP, Fischbach MA, et al. (2017). A gut bacterial pathway metabolizes aromatic amino acids into nine circulating metabolites. Nature 551, 648–652. [PubMed: 29168502]

Donia MS, and Fischbach MA (2015). HUMAN MICROBIOTA. Small molecules from the human microbiota. Science 349, 1254766. [PubMed: 26206939]

Duner P, Al-Amily IM, Soni A, Asplund O, Safi F, Storm P, Groop L, Amisten S, and Salehi A (2016). Adhesion G Protein-Coupled Receptor G1 (ADGRG1/GPR56) and Pancreatic beta-Cell Function. J Clin Endocrinol Metab 101, 4637–4645. [PubMed: 27636017]

Durocher Y, Perret S, Thibaudeau E, Gaumond MH, Kamen A, Stocco R, and Abramovitz M (2000). A reporter gene assay for high-throughput screening of G-protein-coupled receptors stably or transiently expressed in HEK293 EBNA cells grown in suspension culture. Anal Biochem 284, 316–326. [PubMed: 10964415]

Eun CS, Kwak MJ, Han DS, Lee AR, Park DI, Yang SK, Kim YS, and Kim JF (2016). Does the intestinal microbial community of Korean Crohn's disease patients differ from that of western patients? BMC Gastroenterol 16, 28. [PubMed: 26922889]

Fiedorowicz J S. KL. (2004). The Role of Monoamine Oxidase Inhibitors in Current Psychiatric Practice. J Psychiatr Pract 10, 239–248. [PubMed: 15552546]

Fischbach MA (2018). Microbiome: Focus on Causation and Mechanism. Cell 174, 785–790. [PubMed: 30096310]

Glover V S. M; Owen F; Riley GJ. (1977). Dopamine is a monoamine oxidase B substrate in man. Nature 265, 80–81. [PubMed: 834248]

Goodman AL, Kallstrom G, Faith JJ, Reyes A, Moore A, Dantas G, and Gordon JI (2011). Extensive personal human gut microbiota culture collections characterized and manipulated in gnotobiotic mice. Proc Natl Acad Sci U S A 108, 6252–6257. [PubMed: 21436049]

Guo CJ, Chang FY, Wyche TP, Backus KM, Acker TM, Funabashi M, Taketani M, Donia MS, Nayfach S, Pollard KS, et al. (2017). Discovery of Reactive Microbiota-Derived Metabolites that Inhibit Host Proteases. Cell 168, 517–526 e518. [PubMed: 28111075]

Haiser HJ, Gootenberg DB, Chatman K, Sirasani G, Balskus EP, and Turnbaugh PJ (2013). Predicting and manipulating cardiac drug inactivation by the human gut bacterium Eggerthella lenta. Science 341, 295–298. [PubMed: 23869020]

Husted AS, Trauelsen M, Rudenko O, Hjorth SA, and Schwartz TW (2017). GPCR-Mediated Signaling of Metabolites. Cell Metab 25, 777–796. [PubMed: 28380372]

Integrative, H.M.P.R.N.C. (2014). The Integrative Human Microbiome Project: dynamic analysis of microbiome-host omics profiles during periods of human health and disease. Cell Host Microbe 16, 276–289. [PubMed: 25211071]

Irsfeld M, Spadafore M, and Pruss BM (2013). beta-phenylethylamine, a small molecule with a large impact. Webmedcentral 4.

Jutel M, Akdis M, and Akdis CA (2009). Histamine, histamine receptors and their role in immune pathology. Clin Exp Allergy 39, 1786–1800. [PubMed: 20085595]

Kim H, Dwyer L, Song JH, Martin-Cano FE, Bahney J, Peri L, Britton FC, Sanders KM, and Koh SD (2011). Identification of histamine receptors and effects of histamine on murine and simian colonic excitability. Neurogastroenterol Motil 23, 949–e409. [PubMed: 21806740]

Kim SH, Ben-Gigirey B, Barros-Velazquez J, Price RJ, and An H (2000). Histamine and biogenic amine production by Morganella morganii isolated from temperature-abused albacore. J Food Prot 63, 244–251. [PubMed: 10678431]

Kishore A, Purcell RH, Nassiri-Toosi Z, and Hall RA (2016). Stalk-dependent and Stalk-independent Signaling by the Adhesion G Protein-coupled Receptors GPR56 (ADGRG1) and BAI1 (ADGRB1). J Biol Chem 291, 3385–3394. [PubMed: 26710850]

Kroeze WK, Sassano MF, Huang XP, Lansu K, McCorvy JD, Giguere PM, Sciaky N, and Roth BL (2015). PRESTO-Tango as an open-source resource for interrogation of the druggable human GPCRome. Nat Struct Mol Biol 22, 362–369. [PubMed: 25895059]

Larsbrink J, Rogers TE, Hemsworth GR, McKee LS, Tauzin AS, Spadiut O, Klinter S, Pudlo NA, Urs K, Koropatkin NM, et al. (2014). A discrete genetic locus confers xyloglucan metabolism in select human gut Bacteroidetes. Nature 506, 498–502. [PubMed: 24463512]

Le Poul E, Loison C, Struyf S, Springael JY, Lannoy V, Decobecq ME, Brezillon S, Dupriez V, Vassart G, Van Damme J, et al. (2003). Functional characterization of human receptors for short chain fatty acids and their role in polymorphonuclear cell activation. J Biol Chem 278, 25481–25489. [PubMed: 12711604]

Liberles SD, and Buck LB (2006). A second class of chemosensory receptors in the olfactory epithelium. Nature 442, 645–650. [PubMed: 16878137]

Lovenberg W W. H & Udenfriend S (1962). Aromatic amino acid decarboxylase. The Journal of Biological Chemistry 237, 89–93. [PubMed: 14466899]

Lovitt RW, Morris JG, and Kell DB (1987). The growth and nutrition of Clostridium sporogenes NCIB 8053 in defined media. J Appl Bacteriol 62, 71–80. [PubMed: 3571034]

Mavromatis P Q. PC. (2002). ModifiIcation of Niven's Medium for the Enumeration of Histamine-Forming Bacteria and Discussion of the Parameters Associated with Its Use. Journal of Food Protection 65, 546–551. [PubMed: 11899055]

Milshteyn A, Colosimo DA, and Brady SF (2018). Accessing Bioactive Natural Products from the Human Microbiome. Cell Host Microbe 23, 725–736. [PubMed: 29902438]

Nurk S, Bankevich A, Antipov D, Gurevich AA, Korobeynikov A, Lapidus A, Prjibelski AD, Pyshkin A, Sirotkin A, Sirotkin Y, et al. (2013). Assembling single-cell genomes and mini-metagenomes from chimeric MDA products. J Comput Biol 20, 714–737. [PubMed: 24093227]

Oldendorf W (1971). Brain uptake of radiolabeled amino acids, amines, and hexoses after arterial injection. American Journal of Physiology 221, 1629–1639. [PubMed: 5124307]

Özoğul F (2004). Production of biogenic amines by Morganella morganii, Klebsiella pneumoniae and Hafnia alvei using a rapid HPLC method. European Food Research and Technology 219, 465–469.

Palm NW, de Zoete MR, Cullen TW, Barry NA, Stefanowski J, Hao L, Degnan PH, Hu J, Peter I, Zhang W, et al. (2014). Immunoglobulin A coating identifies colitogenic bacteria in inflammatory bowel disease. Cell 158, 1000–1010. [PubMed: 25171403]

Pedersen HK, Gudmundsdottir V, Nielsen HB, Hyotylainen T, Nielsen T, Jensen BA, Forslund K, Hildebrand F, Prifti E, Falony G, et al. (2016). Human gut microbes impact host serum metabolome and insulin sensitivity. Nature 535, 376–381. [PubMed: 27409811]

Perry RJ, Peng L, Barry NA, Cline GW, Zhang D, Cardone RL, Petersen KF, Kibbey RG, Goodman AL, and Shulman GI (2016). Acetate mediates a microbiome-brain-beta-cell axis to promote metabolic syndrome. Nature 534, 213–217. [PubMed: 27279214]

Pezeshki A, Zapata RC, Singh A, Yee NJ, and Chelikani PK (2016). Low protein diets produce divergent effects on energy balance. Scientific Reports 6.

Purcell R H. RA. (2018). Adhesion G Protein–Coupled Receptors as Drug Targets. Annu Rev Pharmacol Toxicol 58, 429–449. [PubMed: 28968187]

Ramachandraih C S. N; Bar KJ; Baker G; Yeragani VK. (2011). Antidepressants: From MAOIs to SSRIs and more. Indian J Psychiatry 53, 180–182. [PubMed: 21772661]

Smith PH, MR; Panikov N; Michaud M; Gallini CA; Bohlooly-Y M; Glickman JN; Garret WS. (2013). The Microbial Metabolites, Short-Chain Fatty Acids, Regulate Colonic Treg Cell Homeostasis. Science 341, 569–573. [PubMed: 23828891]

Smolinska S, Jutel M, Crameri R, and O'Mahony L (2014). Histamine and gut mucosal immune regulation. Allergy 69, 273–281. [PubMed: 24286351]

Sotnikova TD, Budygin EA, Jones SR, Dykstra LA, Caron MG, and Gainetdinov RR (2004). Dopamine transporter-dependent and -independent actions of trace amine beta-phenylethylamine. J Neurochem 91, 362–373. [PubMed: 15447669]

Tan JK M. C; Mariño E; Macia L and Mackay CR. (2017). Metabolite-Sensing G Protein-Coupled Receptors-Facilitators of Diet-Related Immune Regulation. AnnuRevImmunol 35, 371–402.

Thurmond RL, Gelfand EW, and Dunford PJ (2008). The role of histamine H1 and H4 receptors in allergic inflammation: the search for new antihistamines. Nat Rev Drug Discov 7, 41–53. [PubMed: 18172439]

Tyagi P, Mandal MB, Mandal S, Patne SC, and Gangopadhyay AN (2009). Pouch colon associated with anorectal malformations fails to show spontaneous contractions but responds to acetylcholine and histamine in vitro. J Pediatr Surg 44, 2156–2162. [PubMed: 19944226]

Wacker D, Stevens RC, and Roth BL (2017). How Ligands Illuminate GPCR Molecular Pharmacology. Cell 170, 414–427. [PubMed: 28753422]

Williams RM, CDS; Burnett JR. (2008). Phenylketonuria- An Inborn Error of Phenylalanine Metabolism. Clin Biochem Rew 29, 31–41.

Yano JM, Yu K, Donaldson GP, Shastri GG, Ann P, Ma L, Nagler CR, Ismagilov RF, Mazmanian SK, and Hsiao EY (2015). Indigenous bacteria from the gut microbiota regulate host serotonin biosynthesis. Cell 161, 264–276. [PubMed: 25860609]

Highlights

- Screening of gut microbiota metabolomes against hundreds of G protein-coupled receptors
- Phylogenetically diverse gut microbes produce agonists for many GPCRs including orphans
- Bioactivity-based screening reveals diet-microbe-host and microbe-microbe-host axes
- Microbiota-derived GPCR ligands impact local and systemic host physiology

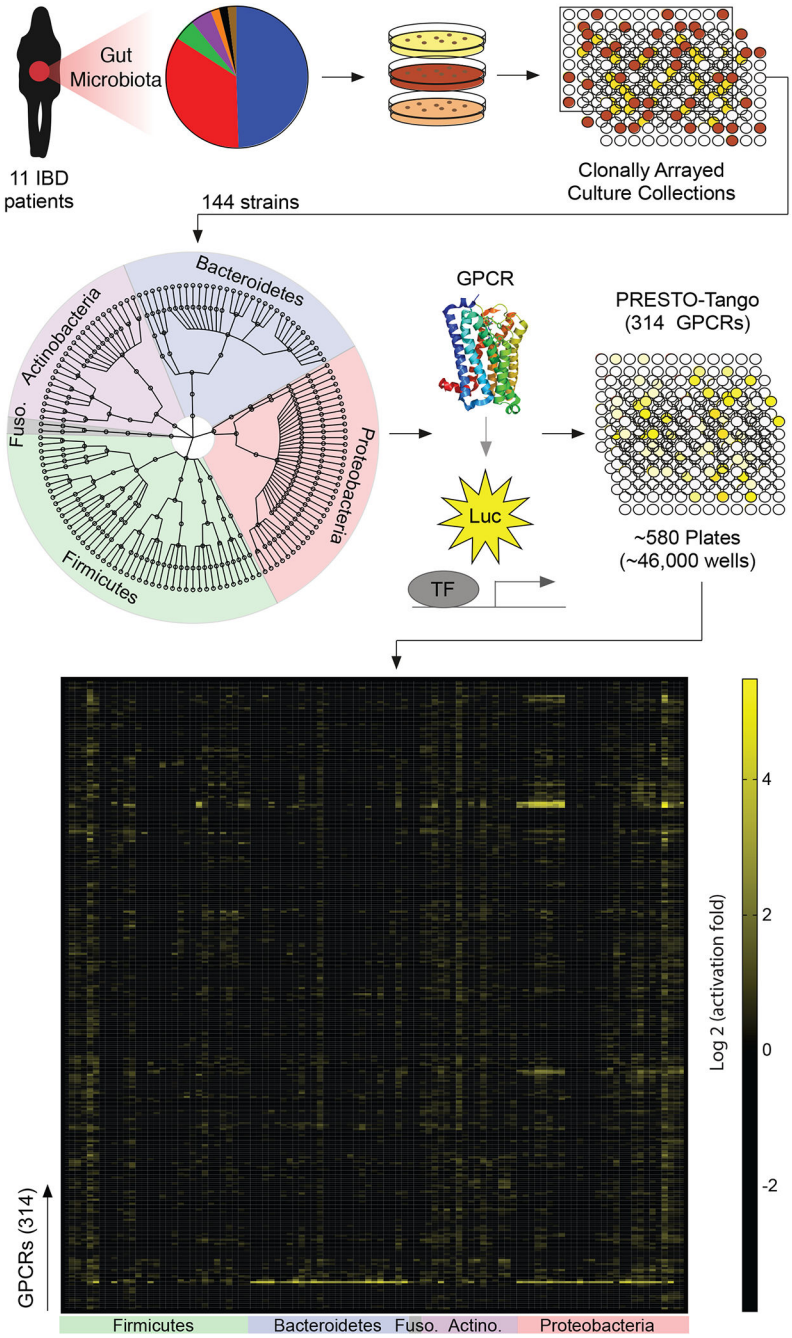

Figure 1. A forward chemical genetic screen identifies human gut microbes that activate GPCRs.

We isolated 144 unique human gut bacteria spanning five phyla, nine classes, eleven orders, and twenty families from 11 inflammatory bowel disease patients via high-throughput anaerobic culturomics and massively barcoded 16S rRNA gene sequencing. Bacterial isolates were grown in monoculture in a medium specialized for the cultivation of human gut microbes (gut microbiota medium) and supernatants from individual bacterial monocultures were screened against the near-complete non-olfactory GPCRome (314 conventional GPCRs) using Parallel Receptor-ome Expression and Screening via Transcriptional Output-Tango (PRESTO-Tango).

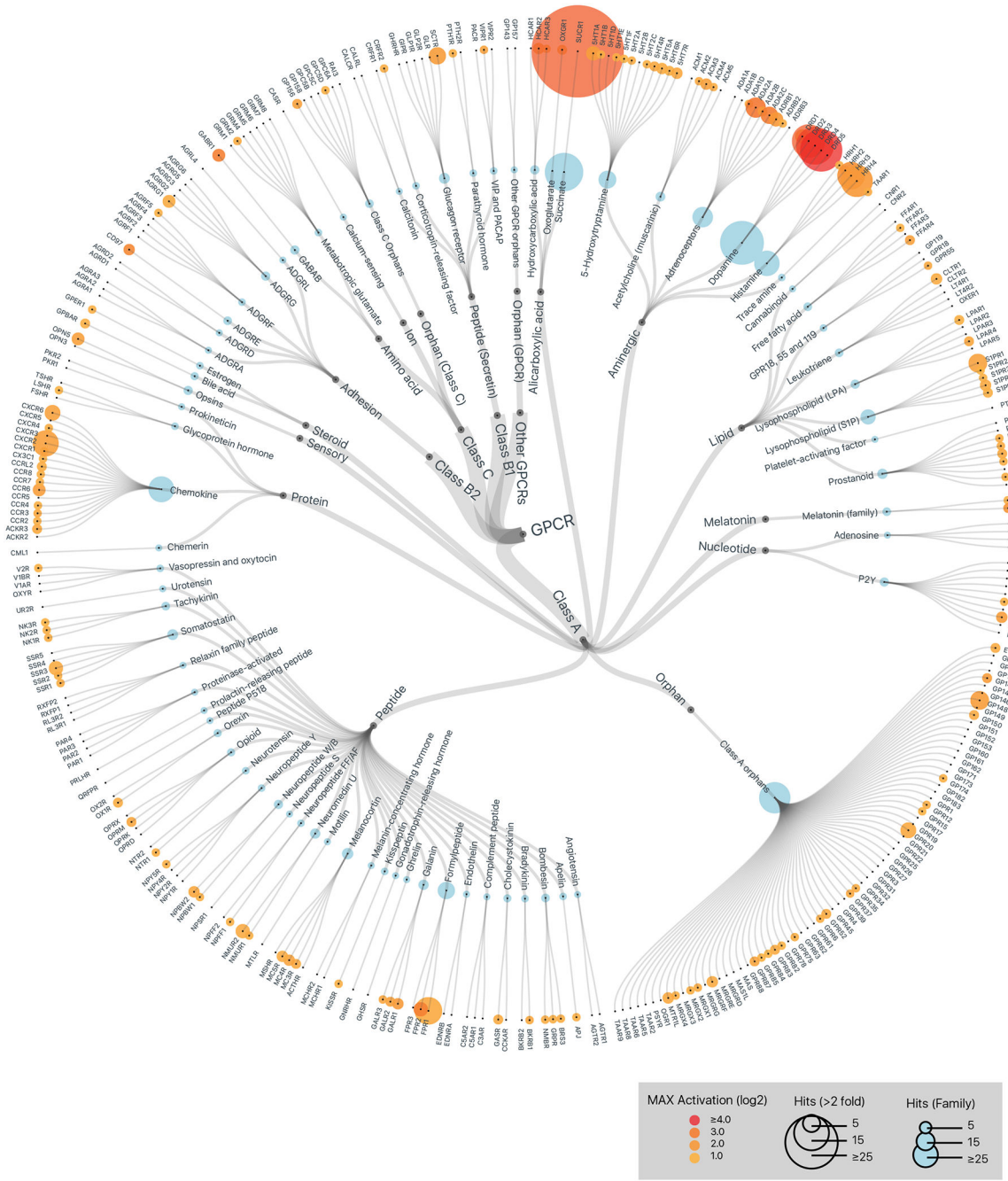

Figure 2. Members of the human gut microbiota produce metabolites that activate diverse human GPCRs.

GPCR activation by metabolomes from a human gut microbiota culture collection consisting of 144 strains isolated from 11 IBD patients. Data is displayed on a hierarchical tree of GPCRs organized by class, ligand type, and receptor family. Color intensity represents the maximum magnitude of activation (log 2) over background (gut microbiota medium alone) across the complete data set. Radii of the circles at each tip represent the number of strains that activated a given receptor or receptor family by more than two-fold over background. Graphics were generated in collaboration with visavisllc using d3.js.

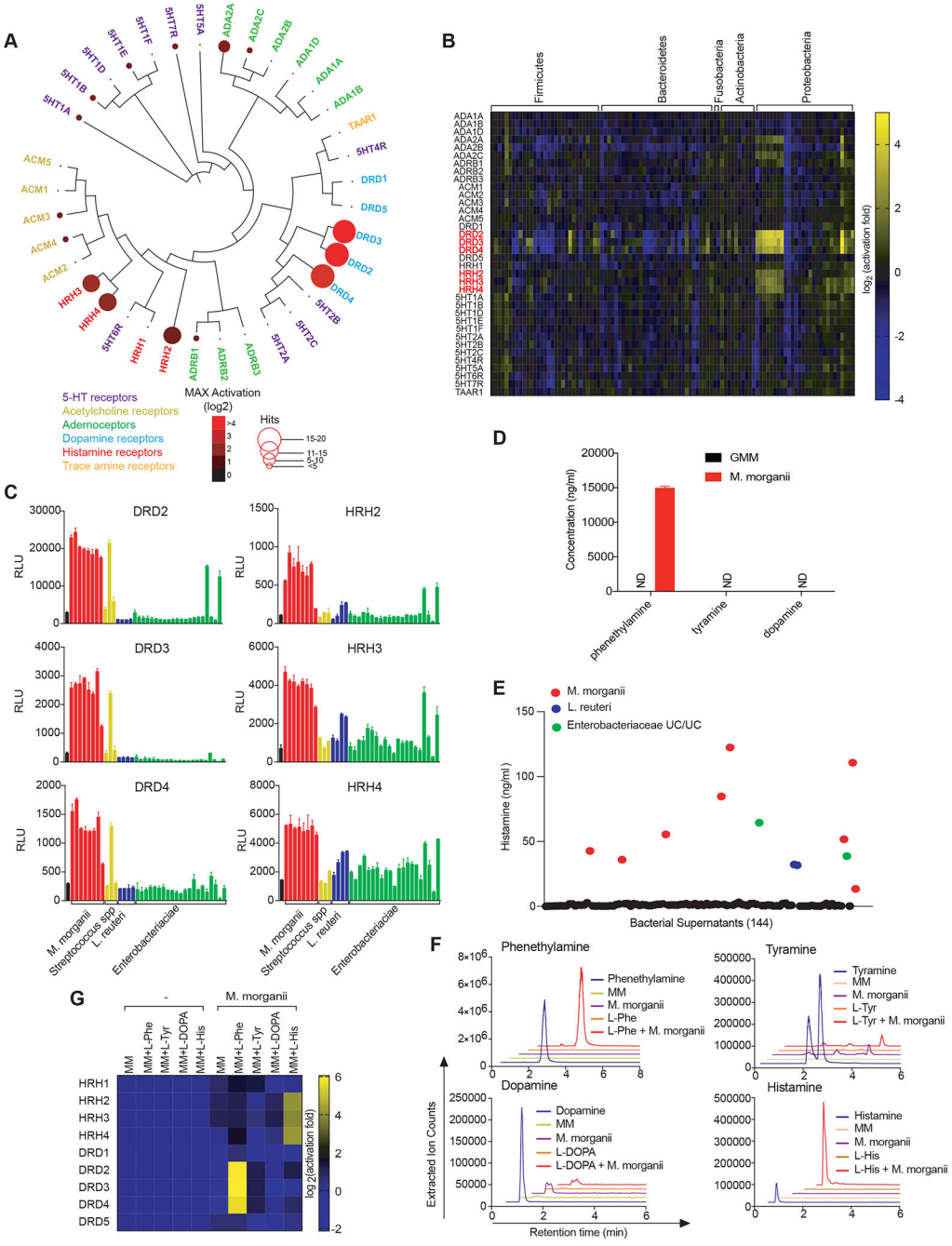

Figure 3. Diverse human gut bacteria activate aminergic GPCRs.

(A) Activation of aminergic GPCRs by metabolomes from a human gut microbiota culture (see Figure 1). GPCR activation was measured by PRESTO-Tango. Screening results are displayed on a phylogenetic tree of aminergic GPCRs. Color intensity represents magnitude of activation over media alone and radii of the circles represents the number of bacteria that activated a given GPCR by more than two-fold over media alone.

(B) Heatmap depicting the activation of aminergic GPCRs by metabolites from a human gut microbiota culture collection as measured by PRESTO-Tango. Fold induction over stimulation with bacterial media alone is depicted on a log2 scale.

(C) Activation of DRD2–4 and HRH2–4 by select species and strains as measured by Tango assays.
(D) Quantification of dopamine, phenethylamine and tyramine production by *M. morganii*. Supernatants from 24-hour cultures of *M. morganii* C135 in gut microbiota medium were analyzed by Triple Quadrupole-Mass Spectrometry (QQQ-MS/MS).
(E) Quantification of histamine production by 144 isolates of human gut bacteria by ELISA (48 hr. cultures).
(F) Mass spectrometric traces of metabolite production by *M. morganii* C135. *M. morganii* was cultured in minimal medium (MM) with or without additional L-Phe, L-His, L-Tyr or L-DOPA for 48 hours. Metabolite production was analyzed by Liquid Chromatography-Mass Spectrometry (LC-MS).
(G) *M. morganii*-derived phenethylamine and histamine activate DRD2–4 and HRH2–4, respectively. *M. morganii* C135 were cultured as described in F and supernatants were screened for activity against DRDs and HRHs by PRESTO-Tango.
Data for all panels other than A and B are representative of at least three independent experiments. Data are presented as mean ± SEM. n=3 replicates per group (C-G).

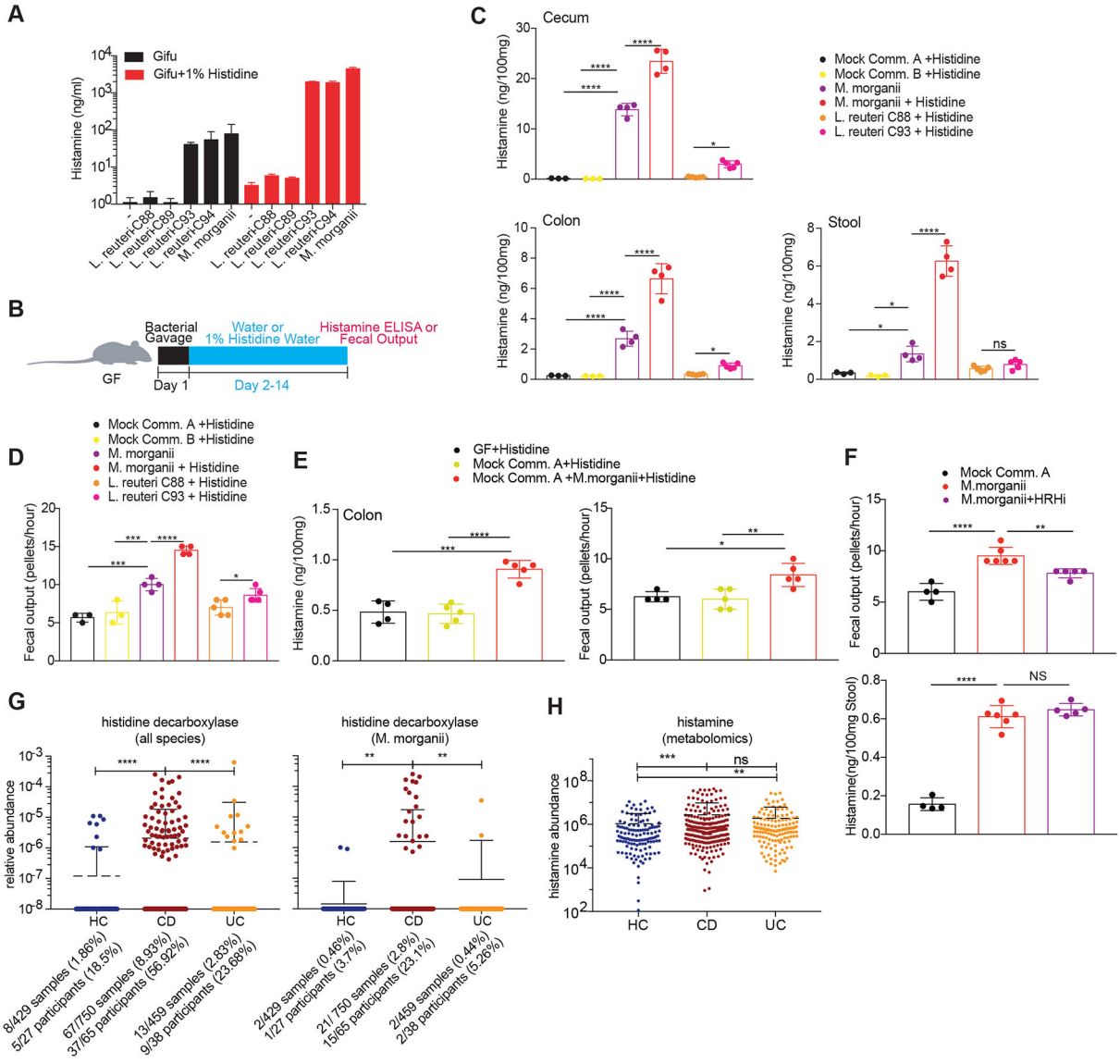

Figure 4. Commensal-derived histamine promotes colon motility.

(A) Production of histamine by *M. morganii* and *L. reuteri*. *L. reuteri* and *M. morganii* strains were cultured in Gifu medium with or without supplemental L-His and histamine concentrations in the supernatants were measured by ELISA after 48 hours (background levels in controls containing supplemental histidine are due to slight cross-reactivity).

(B) Experimental design to test *in vivo* histamine production and the effects of histamine-producing bacteria on colon motility.

(C) *M. morganii*- and *L. reuteri*-derived histamine accumulates *in vivo* in monocolonized mice. Female germ-free C57Bl/6 mice were colonized with mock communities of 9 or 10 phylogenetically diverse human gut bacteria (Mock Community A or B) or monocolonized with *M. morganii* C135, *L. reuteri* C88 or C93. Mice were fed a conventional diet with or without administration of 1% L-His *ad libitum* in the drinking water. Histamine concentrations in cecal and colonic extracts and feces were measured via ELISA. n=3–5 mice per group.

(D) *M. morganii* C135- and *L. reuteri* C93-derived histamine enhances colon motility. Fecal output for mice treated as described in B was measured by counting the number of fecal pellets produced by a single mouse in one hour. n=3–5 mice per group.
(E) *M. morganii* increases colon motility in the context of a mock gut microbial community. Female germ-free C57Bl/6 mice were colonized Mock Community A with or without *M. morganii* C135 and administered 1% L-His *ad libitum* in the drinking water. Histamine concentrations in colonic extracts were measured via ELISA and fecal output was measured as in (D). n=4–5 mice per group.
(F) Histamine receptor inhibition partially reverses the impact of *M. morganii* on colon motility. Female germ-free C57Bl/6 mice were colonized with Mock Community A or monocolonized with *M. morganii* C135 for two weeks. Mice were then treated with or without a cocktail of four histamine receptor inhibitors (targeting HRH1–4) in the drinking water for one week. Histamine concentrations in feces were measured via ELISA and fecal output was measured as in (D). n=4–6 mice per group.
(G and H) Relative abundances of genes encoding histidine decarboxylases (from all bacteria or *M. morganii*) are increased in the microbiomes of patients with Crohn's disease as compared to healthy controls (G). Relative abundance of histamine is increased in IBD patients as compared to healthy controls as measured by metabolomics (H). Data are from longitudinal stool samples from IBD patients publically available from the Human Microbiome Project 2 (iHMP). Total numbers of samples or subjects with detectable *M. morganii* are denoted below each plot; a subject was considered positive if *M. morganii* was detectable in one or more samples from that patient across the complete dataset.
Data in all panels are representative of at least two independent experiments. Data are presented as mean ± SEM. One-way ANOVA with Tukey's post-hoc test (C-F) or Kruskall-Wallis with Dunn's multiple comparisons (G-H), *$p < 0.05$, **$p < 0.01$, ***$p < 0.001$, ****$p < 0.0001$, NS not significant ($p > 0.05$).

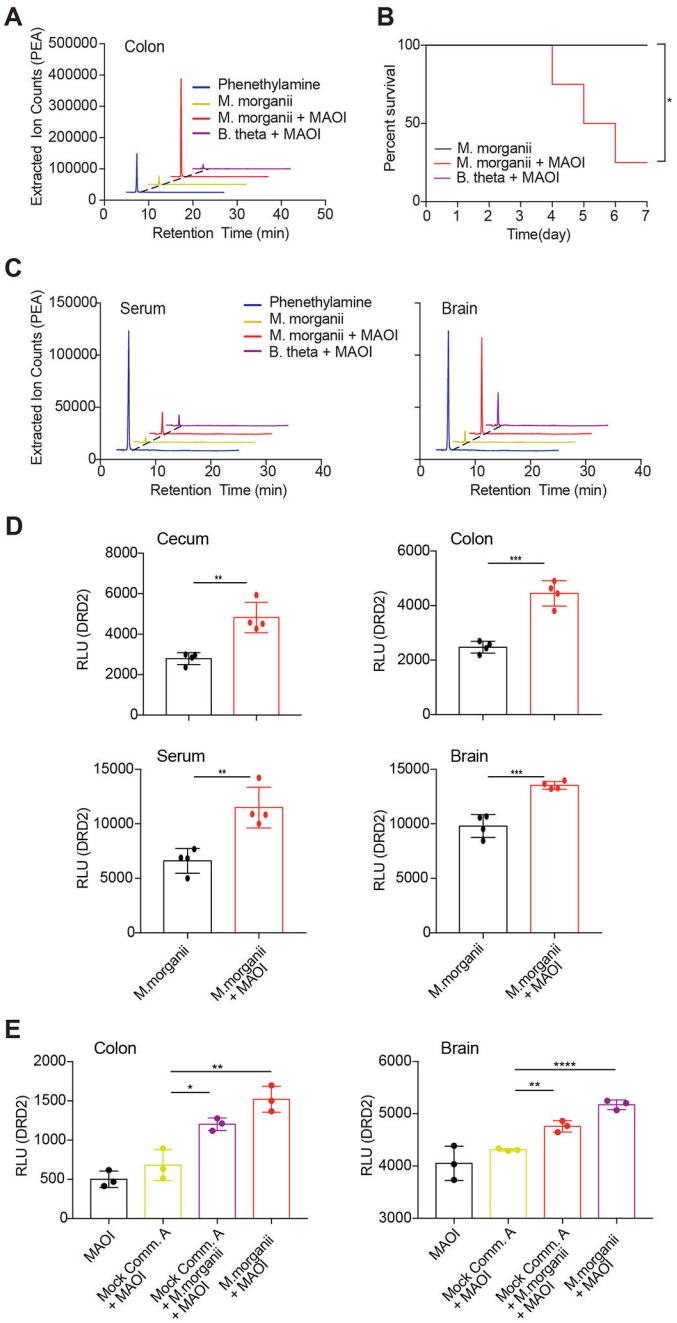

Figure 5. M. morganii-derived phenethylamine combined with MAOI triggers lethal phenethylamine poisoning.

(A) *M. morganii* produces phenethylamine *in vivo*. Female germ-free C57Bl/6 mice were colonized with *M. morganii* C135 and treated with or without the MAOI phenelzine. Phenethylamine concentration in colonic extracts was examined using QQQ-MS/MS.

(B) Mice colonized with *M. morganii* exhibit lethal phenethylamine poisoning after treatment with the MAOI phenelzine. Female germ-free C57Bl/6 mice were monocolonized with *M. morganii* C135 for one week before treatment with phenelzine in the drinking water. Survival is depicted on a Kaplan-Meier curve. n=4 mice per group.

(C and D) *M. morganii*-colonized mice treated with phenelzine accumulated phenethylamine in the cecum, colon, serum and brain. *M. morganii* C135 and *B. theta* C34 monocolonized female C57Bl/6 mice were treated with or without the MAOI phenelzine in the drinking water. Phenethylamine was measured via QQQ-MS/MS (C) or DRD2 PRESTO-Tango (D). n=4 mice per group.

(E) *M. morganii*-derived phenethylamine accumulates in the sera and brains of mice colonized with Mock Community A plus *M. morganii*. Germ-free female C57Bl/6 mice were colonized with Mock Community A with or without *M. morganii* C135, or monocolonized with *M. morganii* C135. All mice were treated with the MAOI phenelzine in the drinking water for one week and phenethylamine accumulation was detected using DRD2-Tango as a proxy.

Data in all panels are representative of at least two independent experiments. Data are presented as mean ± SEM. One-way ANOVA with Tukey's post-hoc test (D-E), Kaplan meier and Log rank analysis (B), *$p < 0.05$, **$p < 0.01$, ***$p < 0.001$, ****$p < 0.0001$.

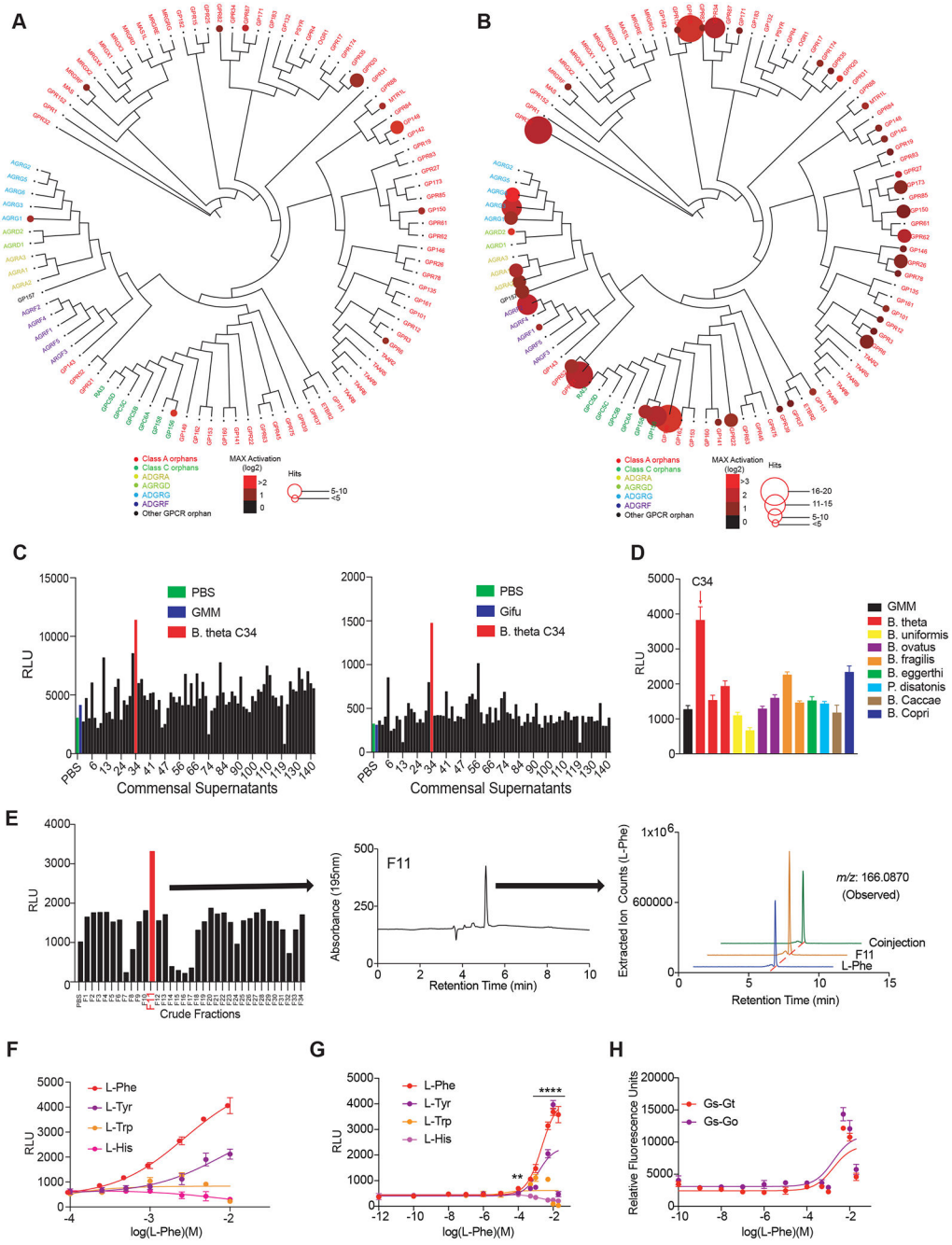

Figure 6. A unique strain of B. thetaiotaomicron C34 is a prolific producer of LPhe and activates GPR56/AGRG1.

(A and B) Activation of orphan GPCRs by metabolomes from a human gut microbiota culture (see Figure 1) grown in gut microbiota medium (A) or Gifu (B) as measured by PRESTO-Tango. Screening results are displayed on a phylogenetic tree of orphan GPCRs that was constructed and visualized with equal branch lengths using gpcrdb.org, PHYLIP and jsPhyloSVG. Color intensities represent the magnitude of activation over media and radii of circles represent the number of bacteria that activated a given GPCR by more than two-fold.

(C) A single isolate C34 assigned to the species *Bacteroides thetaiotaomicron* activates GPR56/AGRG1 when cultured in gut microbiota medium (GMM: top panel) or Gifu medium (bottom panel). Activation of GPR56/AGRG1 by supernatants from 144 human gut isolates was measured via GPR56-Tango.

(D) *B. theta* strain C34 uniquely activates GPR56/AGRG1. Activation of GPR56/AGRG1 by supernatants from diverse species and strains from the genera *Bacteroides* and *Parabacteroides* cultured in GMM was measured via GPR56 PRESTO-Tango.

(E) *B. theta* C34-produced L-Phe activates GPR56/AGRG1. *B. theta* C34 supernatants were fractionated via reversed-phase HPLC and fractions were evaluated for activation of GPR56/AGRG1 via GPR56-Tango. The active fraction (F11) contained a primary constituent that was identified via LC-MS, HRMS-ESI-QTOF, NMR, and advanced Marfey's analyses as LPhe.

(F and G) L-Phe activates the orphan receptor GPR56/AGRG1. Activation of GPR56/AGRG1 by titrating doses of pure L-Phe, L-Tyr, L-Trp, and L-His was measured via GPR56-Tango using RPMI 1640 medium (F) or a custom medium lacking L-Phe and L-Tyr (G).

(H) L-Phe activates G protein-dependent signaling downstream of GPR56/AGRG1 as measured by the CRE-SEAP assay. $G\alpha_s$-$G\alpha_t$ and $G\alpha_s$-$G\alpha_o$ chimeras were used to redirect GPR56/AGRG1 signaling to $G\alpha_s$.

Data in all panels except for A, B, and E are representative of at least three independent experiments. Data are presented as mean ± SEM. One-way ANOVA with Tukey's post-hoc test **$p < 0.01$, ****$p < 0.0001$.

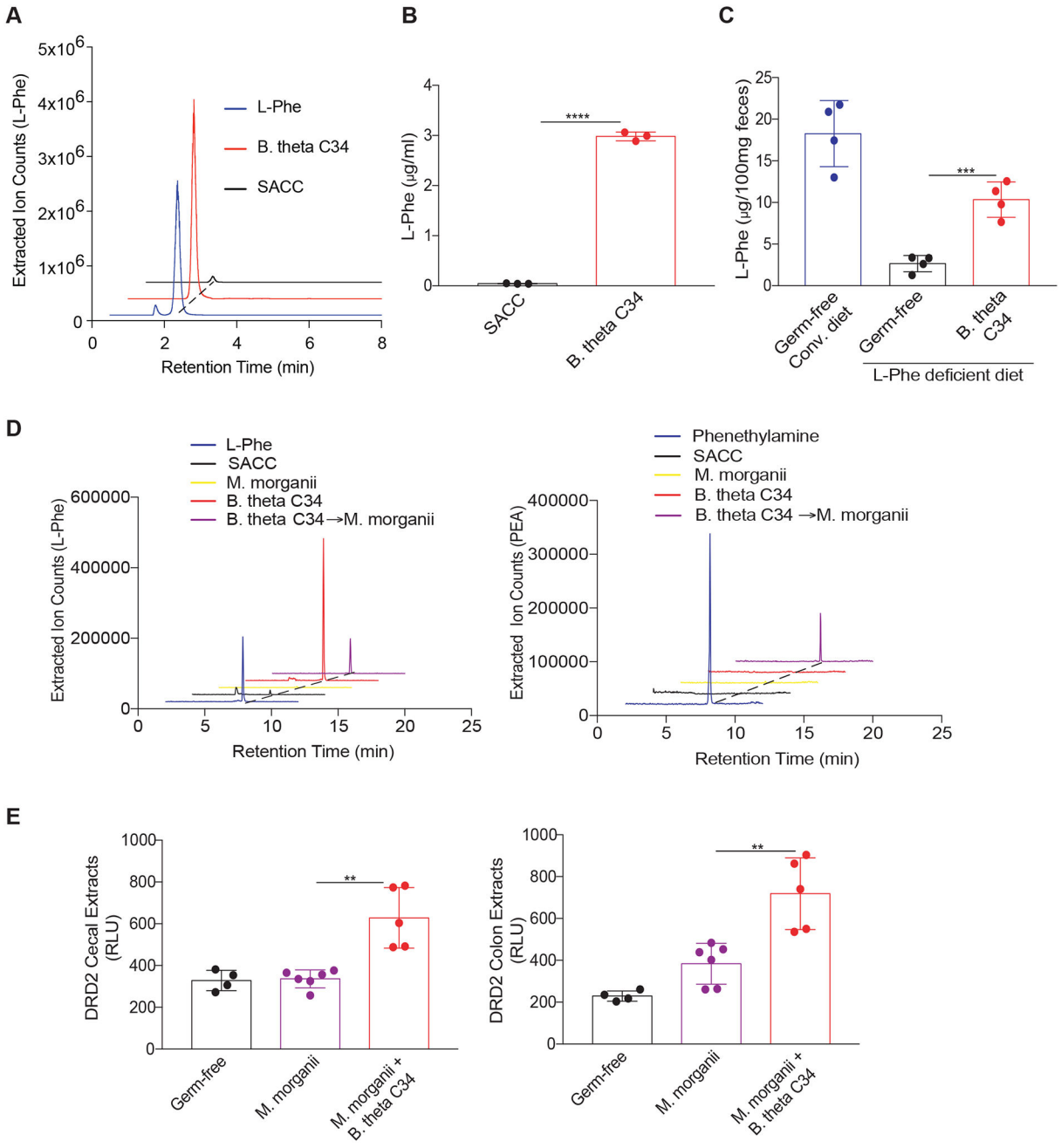

Figure 7. Active metabolic exchange between two commensals supports production of phenethylamine.

(A and B) *B. theta* C34 can directly synthesize L-Phe. L-Phe concentrations in supernatants from C34 grown in a minimal medium (SACC) lacking L-Phe were evaluated by LC-MS (A) and quantitated by QQQ-MS/MS (B).

(C) *B. theta* C34 produces L-Phe *in vivo*. Germ-free female C57Bl/6 mice fed a conventional diet or a defined diet lacking L-Phe were colonized with or without *B. theta* C34. Fecal L-Phe concentrations were measured by QQQ-MS/MS one week after colonization. n=4 mice per group.

(D) *M. morganii* C135 consumes *B. theta* C34-derived L-Phe to produce phenethylamine *in vitro*. *B. theta* C34 cultures grown in SACC medium lacking L-Phe and then incubated with *M. morganii* C135. L-Phe and phenethylamine (PEA) as measured by QQQ-MS/MS.
(E) *B. theta* C34 and *M. morganii* C135 can participate in active metabolic exchange to produce phenethylamine *in vivo*. Germ-free C57Bl/6 mice were monocolonized with *M. morganii* C135 or co-colonized with *B. theta* C34 and *M. morganii* C135, fed a diet lacking L-Phe, and treated with the MAOI phenelzine. Activation of DRD2 by phenethylamine in cecal and colonic extracts was measured by DRD2-Tango. n=4–6 mice per group.
Data in all panels are representative of at least two independent experiments. Data are presented as mean ± SEM. One-way ANOVA with Tukey's post-hoc test (B-C and E-F), **p < 0.01, ***p < 0.001, ****p < 0.0001.

KEY RESOURCES TABLE

REAGENT or RESOURCE	SOURCE	IDENTIFIER
Bacterial and Virus Strains		
B.fragilis	ATCC	Cat# 25285
B.ovatus	ATCC	Cat# 8483
B. thetaiotaomicron	ATCC	Cat# 29741
B.uniformis	ATCC	Cat# 8492
M.morganii	ATCC	Cat# 25830
M.morganii	ATCC	Cat# 49948
Human Gut Microbiota Culture Collections from IBD Patients	Isolated from patients (Palm et al., 2014)	N/A
Chemicals, Peptides, and Recombinant Proteins		
Gifu Anaerobic Broth	VWR	Cat# 11007–214
Desloratadine	Tocris	Cat# 5958
Tiotidine	Tocris	Cat# 0826
Iodophenpropit	Tocris	Cat# 0779
A987306	Tocris	Cat# 3640
Phenethylamine	Sigma-Aldrich	Cat# 241008
Tyramine	Sigma-Aldrich	Cat# T90344
Dopamine	Sigma-Aldrich	Cat# H8502
Histamine	Sigma-Aldrich	Cat# H7129
Acetylcholine	Sigma-Aldrich	Cat# A2661
L-DOPA	Sigma-Aldrich	Cat# D9628
Succinate	Sigma-Aldrich	Cat# 398055
Serotonin	Sigma-Aldrich	Cat# 14927
Gastrin	Sigma-Aldrich	Cat# G9145
Peptide YY	Anaspec	Cat# AS024401
Pancreatic polypeptide	Anaspec	Cat# AS-22866
Cholecystokinin	Sigma-Aldrich	Cat# C2175
Trace mineral supplement	ATCC	Cat# MD-TMS
Vitamin supplement	ATCC	Cat# MD-VS
L-glycine	Sigma-Aldrich	Cat# G8898
L-valine	Sigma-Aldrich	Cat# 94619
L-leucine	Sigma-Aldrich	Cat# L8000
L-isoleucine	Sigma-Aldrich	Cat# 12752
L-methionine	Sigma-Aldrich	Cat# 64319
L-histidine	Sigma-Aldrich	Cat# H8000
L-arginine	Sigma-Aldrich	Cat# A5131
L-phenylalanine	Sigma-Aldrich	Cat# P2126
L-tyrosine	Sigma-Aldrich	Cat# T3754

REAGENT or RESOURCE	SOURCE	IDENTIFIER
L-tryptophan	Sigma-Aldrich	Cat# T0254
N-methylphenethylamine	Sigma-Aldrich	Cat# M68423
Octopamine	Sigma-Aldrich	Cat# O0250
Synephrine	Sigma-Aldrich	Cat# S0752
Epinephrine	Sigma-Aldrich	Cat# E4250
Norepinephrine	Sigma-Aldrich	Cat# A7257
3-Methoxytyramine	Sigma-Aldrich	Cat# M4251
DMEM	Sigma-Aldrich	Cat# D6429
RPMI 1640	Thermo Fisher	Cat# 21870092
D-phenylalanine	Sigma-Aldrich	Cat# 673-06-3
FDAA (Marfey's Reagent)	Thermo Fisher	Cat# 48895
Critical Commercial Assays		
Bright-Glo™Luciferase Assay System	Promega	Cat# E2620
Histamine Elisa Kit	Enzo Life Sciences	Cat# ENZ-KIT140-0001
Deposited Data		
Shotgun whole-genome sequencing data	This paper	PRJNA512876
iHMP metabolome data	NIH Integrative Human Microbiome Project (Integrative, 2014)	https://ibdmdb.org/tunnel/public/HMP2/Metabolites/1723/products
iHMP metagenome data	NIH Integrative Human Microbiome Project (Integrative, 2014)	https://ibdmdb.org/tunnel/public/HMP2/Metabolites/1723/products
M. morganii whole genomes (previously deposited)	NCBI	https://www.ncbi.nlm.nih.gov/genome
Experimental Models: Cell Lines		
HTLA cells	(Barnea et al., 2008)	N/A
HEK293T	ATCC	Cat# CRL-3216
Experimental Models: Organisms/Strains		
Germ-free C57Bl/6 mice	University of Michigan Gnotobiotics Center	https://microbe.med.umich.edu/services/germ-free-gnotobiotic-mouse-facilities
Recombinant DNA		
PRESTO-Tango Plasmids	Addgene; (Kroeze et al., 2015)	Kit #1000000068
$G\alpha_s$-$G\alpha_t$ and $G\alpha_s$-$G\alpha_o$ chimeras	(Liberles and Buck, 2006)	N/A
CRE-SEAP reporter plasmid	(Liberles and Buck, 2006)	N/A
Software and Algorithms		
QIIME2 2018.8	QIIME 2 development team, 2018	https://qiime2.org/
DADA2 (QIIME2 plugin)	(Callahan et al., 2016)	http://benjjneb.github.io/dada2/
Trimmomatic v.0.38	(Bolger et al., 2014)	http://www.usadellab.org/cms/?page=trimmomatic
SPAdes 3.13.0	(Bankevich et al., 2012; Nurk et al., 2013)	http://cab.spbu.ru/files/release3.13.0/manual.html

REAGENT or RESOURCE	SOURCE	IDENTIFIER
RAST server	(Aziz et al., 2008)	http://rast.nmpdr.org/rast.cgi?page=Jobs
BBMap	DOE Joint Genome Institute	https://sourceforge.net/projects/bbmap/
Other		
600 MHz NMR system with a cryoprobe	Agilent	N/A
iFunnel 6550 ESI-HRMS-QTOF	Agilent	N/A
1260 Infinity system	Agilent	N/A
Prepstar HPLC	Agilent	N/A
Anaerobic Chambers	Coy	Custom built
Spectramax i3x plate reader	Molecular Devices	I3X
Gnotobiotic isolators	Class Biologically Clean	N/A
Isocage P Microisolator Caging System	Techniplast	ISO72P